Project Narrative

Company Name and Address: Particle Beam Lasers, Inc.
18925 Dearborn Street, Northridge, CA 91324-2807

Principal Investigator: Robert J. Weggel

Project Title: Study of a Final Cooling Scheme for a Muon Collider Utilizing High-Field Solenoids --- Cooling Simulations and the Design, Fabrication & Testing of Coils to Advance the Technology for a 50-Tesla Magnet

Topic 49: Advanced Concepts and Technology for High Energy Accelerators

Subtopic (b): Novel Devices and Instrumentation Development

Contents

I) Significance, Background Information, and Technical Approach

a) Introduction

The U.S. Department of Energy is interested in the development of novel devices and instrumentation for use in producing intense muon beams suitable for muon colliders and for other applications. A Muon Collider might allow the study of High Energy Physics at energies higher than practical with more conventional technologies. Such a facility would be much smaller than conventional High Energy Physics facilities such as proton-proton colliders (such as the LHC [ref 1]), or electron positron colliders (such as the ILC [ref 2] or CLIC [ref 3]). Figure 1 illustrates this advantage showing, on the same scale, the LHC, ILC, CLIC, and a Muon Collider. The energies given are the center-of-mass energies for the electron or muon colliders, where the full particle energies are available. For the proton-proton case the energy given is the approximate energy in the individual parton-parton collisions that are available for high energy physics studies. Muon colliders allow the high energy study of point-like collisions of leptons without some of the difficulties associated with high energy electrons, such as the synchrotron radiation requiring their acceleration to be essentially linear and, for this reason, long. Muons can be accelerated in smaller rings and offer other advantages, but they are produced only diffusely and they decay rapidly, making the detailed design of such machines difficult.

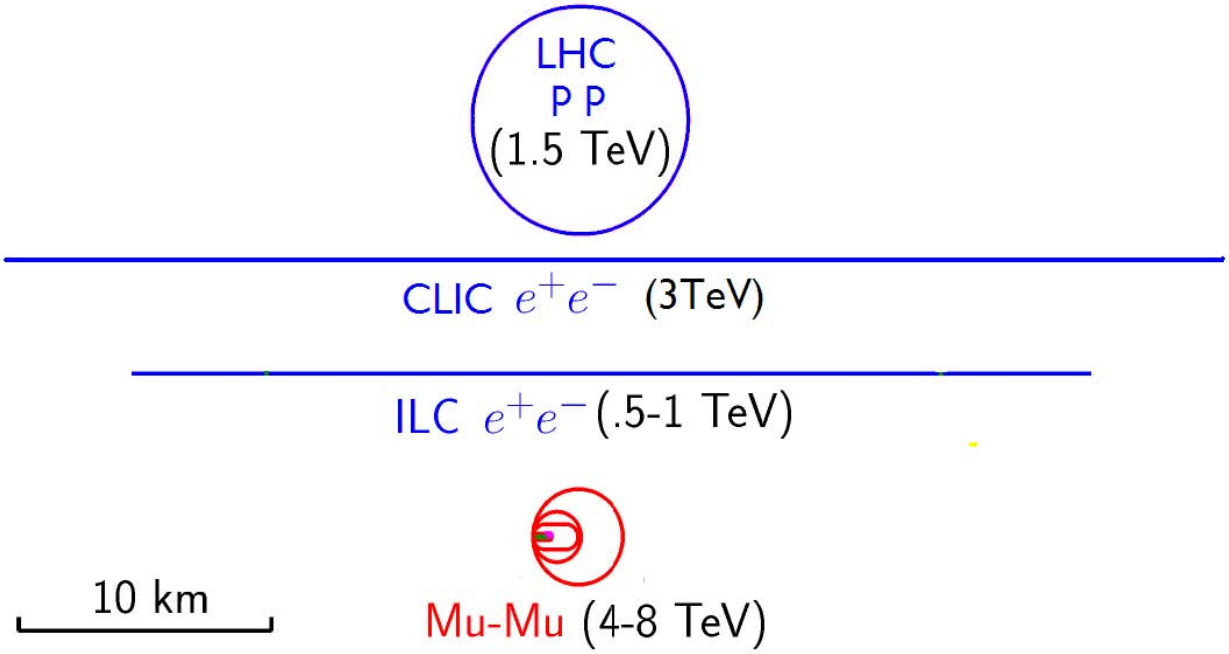

Figure 1: Relative sizes and effective available energies of High Energy Physics facilities

There are two significant technical challenges in the development of the required intense muon beams. The first is the production and collection of the muons and the second is the reduction of the phase space (cooling) of the muon beam in order to obtain the required beam properties. Such cooling involves the reduction of the beam's extent in 6-D phase space, i.e. in each of the three space and three momentum dimensions. The only technique that is fast enough for muon beam

cooling is ionization cooling [ref 4]. In this process, the magnitudes of 3-dimensional momentum vectors of the muon particles are reduced via energy loss in an ionizing media, followed by the subsequent restoration of only the longitudinal momentum component with rf power.

In this proposal we would carry out a study of the use of very high field solenoids for the final muon cooling for muon colliders. The required low emittances can be obtained by passing the muons, at low energies, through liquid hydrogen inside the very high field solenoids. The cooling would be performed in a modest number (7-12) of solenoids, between which the muons would be re-accelerated and phase rotated. The study is innovative because no such optimization of a sequence has yet been performed. Another innovative approach that would be studied is the bending of the muons between solenoids so that each solenoid is used a number of times, thus reducing their total number, cost and total power consumption.

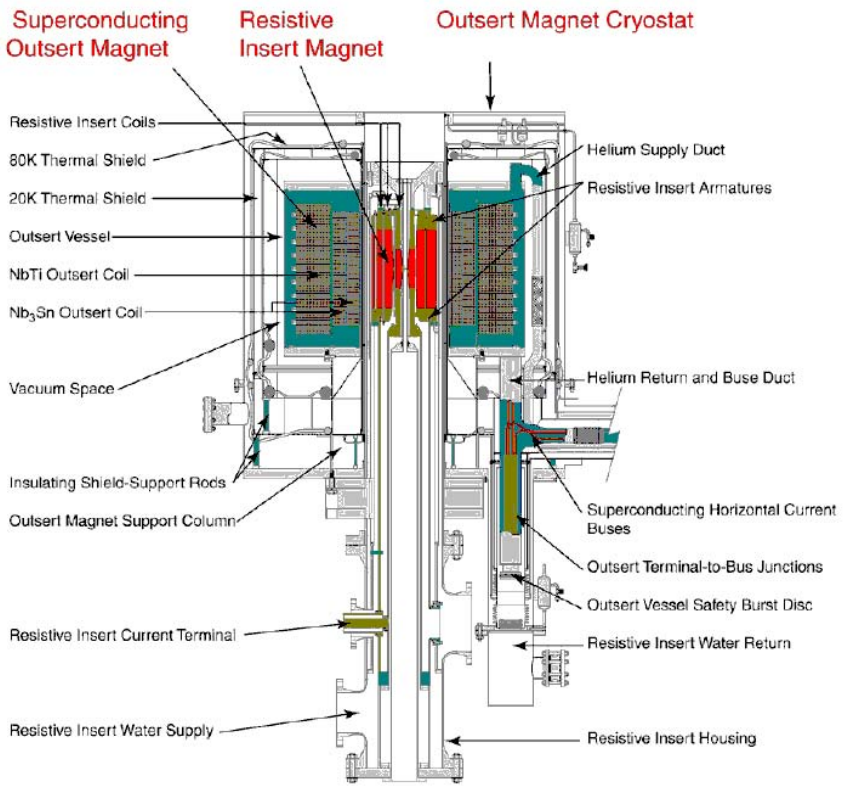

Figure 2: Cross section of the NHMFL 45 T DC hybrid solenoid

A second part of the project would study the re-optimization of the required very high field (45-50 T) hybrid solenoids with specifications adapted to the specific needs of muon cooling as defined in the first part of the study. The work would start from the design of the existing 45T solenoid [ref 5] currently in operation at the National High Magnetic Field Laboratory (NHMFL) in Tallahassee, Florida, and shown in Figure 2. The study would consider possible design modifications to this magnet in view of specific requirements for this application. The work would include a study of raising the field fraction contributed by superconducting coils and reducing the fraction from resistive coils, in order to reduce the power consumption of such magnets (30 MW for the NHMFL 45 T magnet). The main innovation in this part of the study is the optimization of this technology to

this specific innovative application.

b) A Cooling Scenario for Muon Colliders

Introduction

Muon colliders were first proposed by Budker in 1969 [ref 6], and later discussed by others [ref 7]. A more detailed study was done for Snowmass 96 [ref 8], but in none of these was a complete scheme defined for the manipulation and cooling of the required muons.

The specific design, simulation, and optimizations proposed for this study would be done in the context of the only published complete scheme for production and cooling a muon beam for muon colliders [ref 9]. The parameters of three specified muon colliders were presented, and a complete production and cooling scenario described.

The scheme starts with the front end of a proposed neutrino factory [ref 10] that yields bunch trains of both muon signs. Six dimensional cooling, using emittance exchange, in gentle helical RFOFO (Reverse FOcus FOcus) lattices, reduces the longitudinal emittance until it becomes possible to merge the trains into single bunches, one of each sign. Further cooling in all dimensions is applied to the single bunches in further gentle helical RFOFO lattices. Final transverse cooling to the required parameters is achieved in 50 T solenoids. Preliminary simulations of each element have been done at some level.

We will first describe the components of this system and then discuss the problems in the final cooling whose solution this study would address.

Collider Parameters and Cooling Scenario

Table 1: Parameters of two Muon Colliders using the same capture and cooling scenario.

E(center of mass)	(TeV)	1.5	4
Luminosity	(10^{34} cm^2 sec^{-2})	1	4
Beam-beam tune shift		0.1	0.1
Muons per bunch	(10^{12})	2	2
Average ring bending field	(T)	5.2	5.2
Focus parameter beta	(mm)	10	3
Rms fractional momentum spread	(%)	0.09	0.12
Fractional transmission from capture to ring		0.07	0.07
Repetition Rate	(Hz)	13	6
Proton Driver Power	(MW)	4	1.8
Transverse emittance in ring	(pi mm mrad)	25	25
Longitudinal emittance in ring	(pi mm mrad)	72,000	72,000

Table 1 gives parameters for muon colliders at two energies. Those at 1.5 TeV correspond to a recent collider ring design [ref 11]. The 4 TeV example is taken from the 96 Study [ref 8]. Both use the same muon intensities and emittances, although the repetition rates for the higher energy machines are reduced to control neutrino radiation.

Figure 3a shows a schematic of the components of the system. Figure 3b shows a plot of the longitudinal and transverse emittances of the muons as they progress from production to the specified requirements for the colliders. The subsystems used to manipulate and cool the beams to meet these requirements are indicated by the numerals 1-9 on the figures.

Muon Production

The muons are generated by the decay of pions produced by proton bunches interacting in a mercury jet target [ref 12]. These pions are captured by a 20 T solenoid surrounding the target, followed by an adiabatic lowering of the field to a decay channel.

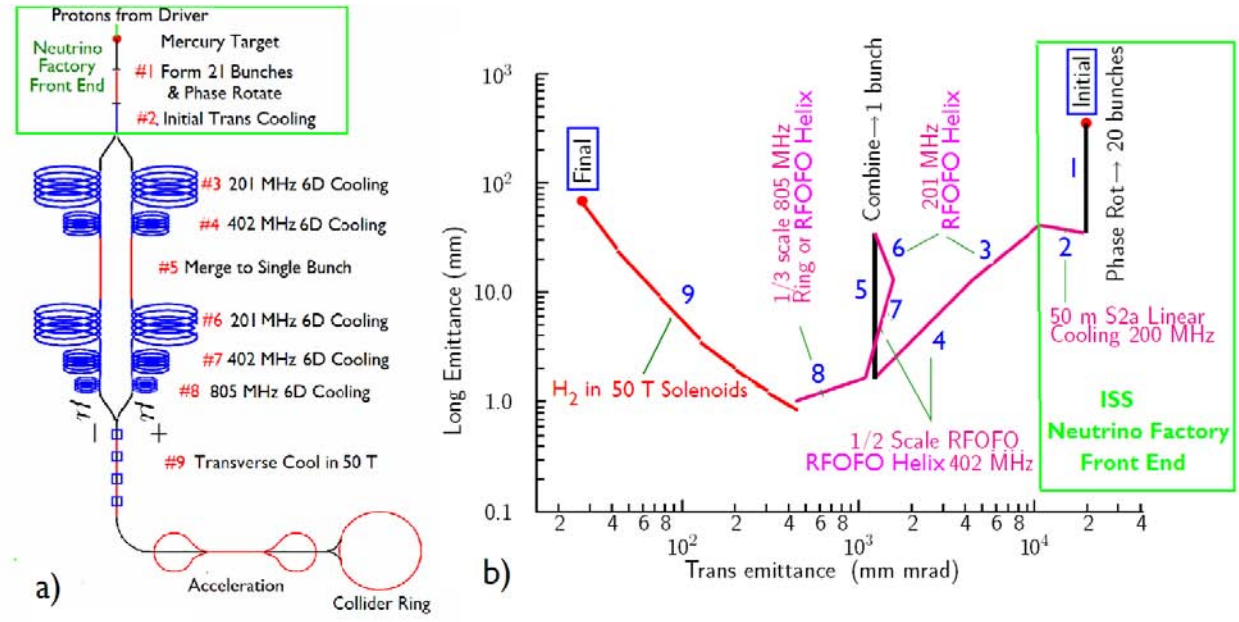

Figure 3: Proposed complete Scheme for a Muon Collider: a) Muon Collider Schematic b) Plot of longitudinal emittance vs. transverse emittance for each of the step.

Final transverse cooling in high field solenoids

It is the continued design and optimization of this part of the system that this second phase of the proposed study would be devoted to.

At the end of stage #8 the transverse emittance is about one order of magnitude greater than required, but the longitudinal emittance is about two orders of magnitude less, i.e. better, than that required. This low longitudinal emittance allows us to do the final cooling in a channel without dispersion or wedges: a channel that cools only in the transverse direction and allows the longitudinal emittance to rise.

To attain the required final transverse emittance, the cooling needs stronger focusing than is practical with 6D cooling lattices. But higher fields are possible in a linear channel that cools only in the transverse dimensions. The higher the field, the lower the equilibrium emittance; and since the lowest possible emittance is desirable, we propose the use of the highest available DC magnetic fields. The highest DC magnet in the world is the 45 T hybrid solenoid [ref 5] at the National High Magnetic Field Laboratory (NHMFL) in Florida. Since this magnet has been operating for some time, and improvements in technologies, such as high temperature superconductors (HTS) have occurred since, it has been assumed that DC fields of 50 T should be possible, and have used this value in preliminary studies [ref 13].

The cooling would occur in a liquid hydrogen pipe on the axis of the solenoid. But for muons near their ionization minimum (approximately 300 MeV/c), even a 50 Tesla field cannot focus the muons tightly enough to reach our desired final emittance. However, if the momentum is allowed to fall to ~30 MeV/c, then the resulting increased focusing strength, combined with the greater energy loss rate, allows one to reach the requirement. Operating at such a low momentum has the disadvantage that the energy loss rate is rising rapidly with falling energy, resulting in a rapid increase in the energy spread and thus the longitudinal emittance. However, as we have noted above, the earlier 6D cooling has lowered the longitudinal emittance to a value far below that needed. So the rise in longitudinal emittance, resulting from cooling at such a low momentum, can be tolerated.

The preliminary study of the complete scenario [ref 9] simulated the individual 50 T cooling stages down to the required emittances, but those simulations did not include losses or emittance dilutions in required matching sections, and assumed Gaussian distributions of muons at the start of each stage, rather than the non-Gaussian distributions that are produced by the previous stage. It is by no means clear that, when such effects are included, the required cooling sequence can be made to work. This proposed study would address these questions using whatever tools prove necessary. In addition, the study would address the specific magnet requirements for each stage and study those modifications needed to the existing NHMFL magnet design to meet these requirements. The study would also look at how the designs might be optimized, perhaps by including the use of HTS materials.

Ongoing Related Work on Muon Collider Cooling

a) The required rf in the current RFOFO 6D cooling systems operate in significant magnetic fields. There is a question as to whether the specified gradients of rf cavities operating under vacuum would operate in those fields. This is under study by the MuCOOL collaboration [ref 16] and alternative designs using high pressure hydrogen gas, or open cell rf with solenoids in the irises are being considered.

b) Instead of the gentle helical RFOFO lattices for 6D cooling described here, a planar wiggler lattice is being studied [ref 17]. Such a lattice would cool both muon signs simultaneously, thus greatly simplifying the system.

c) Another alternative to the gentle helical RFOFO 6D cooling lattices are high pressure hydrogen filled Helical Cooling Channels (HCC) [ref 18]. The realistic integration of rf into these channels remains to be defined, but, given such integration, they could be a valid alternative to the RFOFO

lattices.

d) Theoretical studies [ref 19] have suggested an alternative to the use of the very high field solenoids for the final cooling. Indeed, these theoretical studies suggest cooling to significantly lower final transverse emittances than discussed here. But no lattice that achieves the required parameters has been defined, and the problem seems very hard.

e) In addition, many other details need designing and simulating, and the various new technologies (mercury target, ionization cooling, helical lattice, high field solenoids, etc.) need demonstrating.

c) Introduction to Muon Cooling in 50 T Solenoids

Figure 4 shows the concept of 2 stages of the final cooling sequence. The cooling takes place in small diameter liquid hydrogen absorbers inside the very high field (50 T) solenoids. Matching is required between the 50 T magnet and a lower (of the order of 1 T) field beam transport. This beam transport consists of a drift length, phase rotation and reacceleration. The drift allows the bunch to grow in length. The rf must correct the resulting time-energy correlation and reaccelerate the muons to the energy required for the following stage. In some, but not all, cases there is also a field reversal somewhere in the transport.

Figure 5 shows an example of some parameters for 8 stages of cooling in 50 T solenoids. The changes in parameters in each stage were obtained by separate simulations in ICOOL [ref 14], but the lines joining each stage do not represent simulations, but provide the specifications of the as not yet designed matching and re-acceleration between the stages.

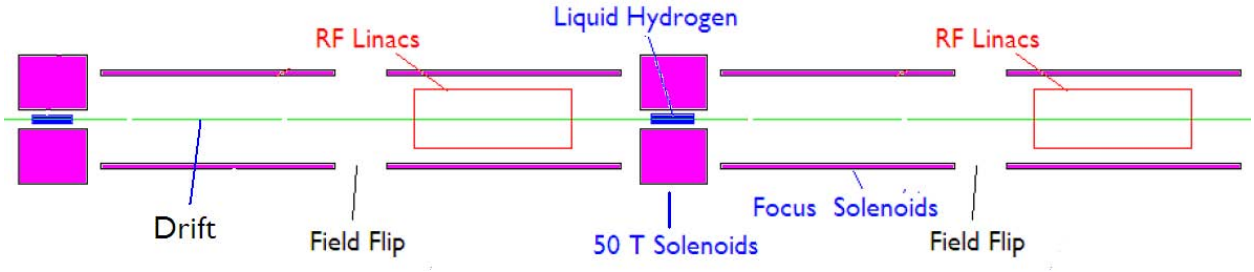

Figure 4: Schematic of two stages of 50 T solenoid final cooling.

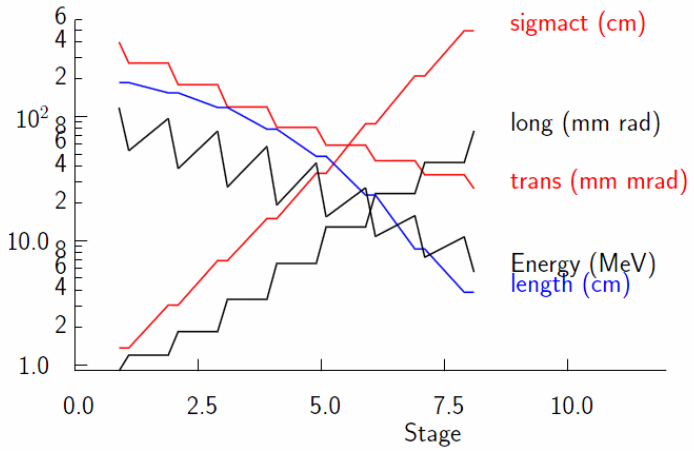

Figure 5: Some starting parameters as a function of stage.

After all 8 stages, the transverse emittance is seen to fall from its initial value of 400 mm mrad (as obtained from ICOOL simulations of an RFOFO 6D cooling lattice) to the required value of 25 mm mrad. In each stage, the energy is seen to drop in the absorber and then increase in the following re-acceleration. But the reacceleration is always a little less than the loss in the absorber so that the mean energy falls, thus assuring stronger focusing in each successive stage. After each stage, the relative momentum spread has risen because of the falling energy and rising longitudinal emittance. The following matching system must reduce this momentum spread to an appropriate value by a phase rotation that increases the bunch length. It is seen in figure 5 that these bunch lengths, starting at a few cm, rise to about 500 cm at the end.

II) Degree to which Phase I has Demonstrated Technical Feasibility

a) Design and Simulation of Cooling in 50 T Solenoids

Initial attempts to simulate matching from one solenoid cooling stage to the next

An attempt was made, as specified in the Phase I proposal, to simulate the sequence of stages using matrixes to perform in the initial sequence of solenoids, shown in Figure 5. The final energy was so low that the bunches grew to 500 cm. This required a rather long drift prior to the rf re-acceleration and suffered significant muon loss from decay. It was realized that this loss could be reduced if somewhat higher energies and shorter bunches were used. The modified sequence would now end with two 50 T magnets, each with 20 cm long hydrogen absorbers. Both stages could then use the same magnet design discussed in section b) Figure 17b.

We were unable to achieve matching between any two magnets using a linear matrix transformation. In all cases such a linear phase space transformation resulted in significant (~30%) longitudinal emittance growth.

An attempt was then made to design and simulate matching and re-acceleration using the code ICOOL [ref 15]. 1000 muons were generated with Gaussian distributions in all coordinates, emittances specified from analytic considerations, and beam betas and angular momenta chosen to match into the initial transport. For this first attempt, it was assumed that the wave forms, being

generated by induction accelerators, would have rf waveforms consisting of flat or linearly changing gradients. The rf gradients were limited to a maximum of 1 MeV/m and the lengths and gradient slopes allowed to vary. As in the matrix case, no solution was found that did not result in significant (of order 30%) longitudinal emittance growth. The reason, in both cases, appeared to be related to the non-linearity of the energy loss mechanism (there is a low energy Landau tail), and/or by the essential non-linearity in the transformation from energy to velocity of the muons.

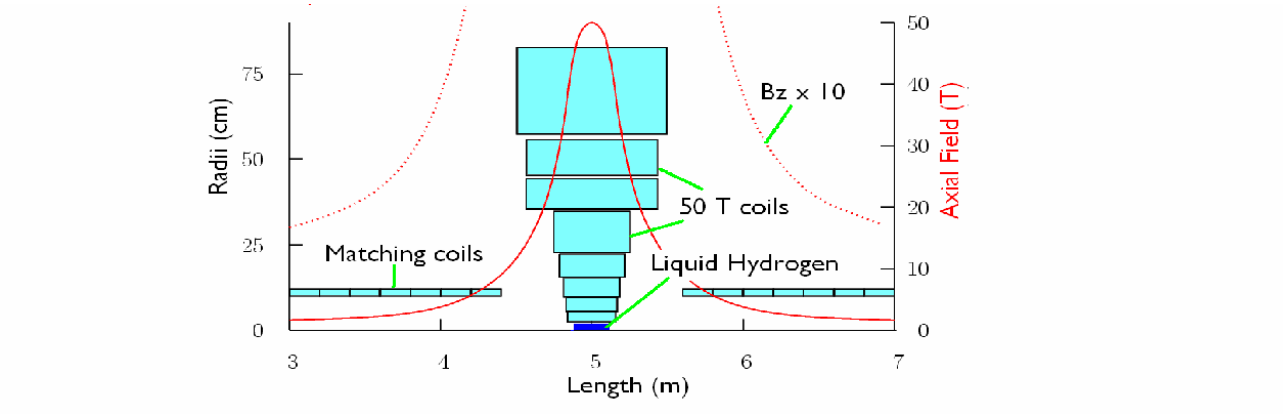

Figure 6: Coil dimensions of 50 T magnet, the matching solenoids and liquid hydrogen pipe. The solid red line shows the axial fields and the dotted shows these scaled up by 10.

Successful demonstration of matching in and out of a 50 T solenoid

Finally, matching was attempted allowing the rf to have non linear time dependence. Specifically, sinusoidal wave forms were tried. With this added flexibility, good matching between the final two stages was achieved. Since the waveforms were sinusoidal, it might be assumed that resonant rf acceleration would now be preferred, but the frequencies were so low and the pulses so relatively short (see Figure 9), that Induction Acceleration would still be the preferred method of achieving the wave forms.

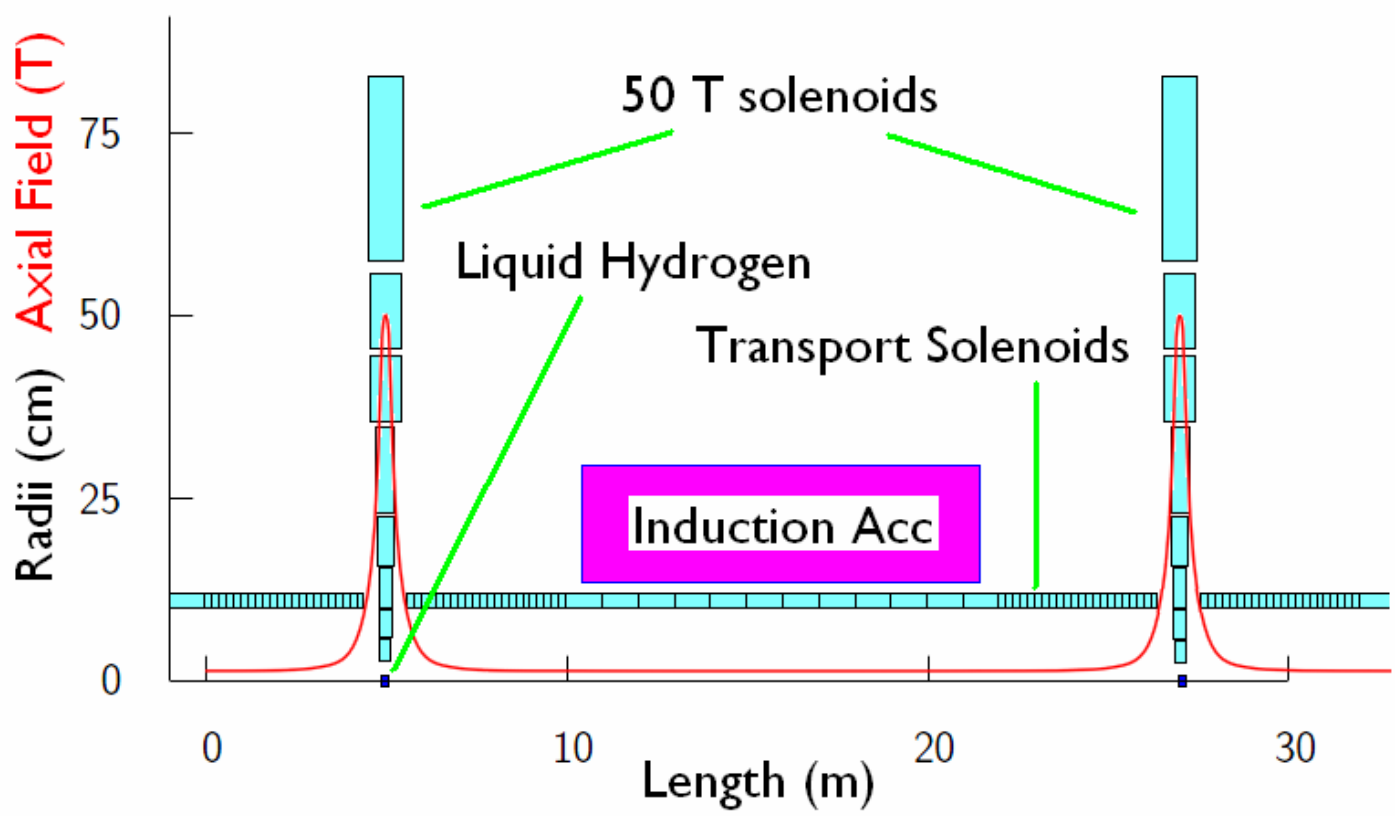

Figure 7: The two final 50 T magnets, the matching coils and re-acceleration Induction Linac.

Figure 6 shows the coils of the 50 T solenoid together with the nearby matching coils and the axial magnetic fields from both. The magnet design used in this work is the all-superconducting solution defined in Figure 17b. Sequences of 20 cm diameter coils placed before and after each 50 T solenoid have been designed to match the transverse phase space from the high field solenoid to a sequence of low field (approximately 1 T) solenoids that transport the beam to and through the rf systems. The match from the 50 T solenoid to the transport was achieved by a gentle change of the field that satisfied the condition that $d\beta/dx < 25\%$. Table 2 gives the parameters of this sequence of matching solenoids, together with those for the 50 T solenoids.

Matching from one solenoid stage to the next

Figure 7 shows the optimized design for the matching and re-acceleration between the penultimate and final 50 T solenoids. The solenoids under the induction units would need to have gaps as in the Study II design (see Figure 8). The solenoids in that design had a larger inside radius (60 cm) than those for the present design (20 cm). The core cross sections would also be smaller because both specified gradients and pulse lengths are less. But the general features would be similar.

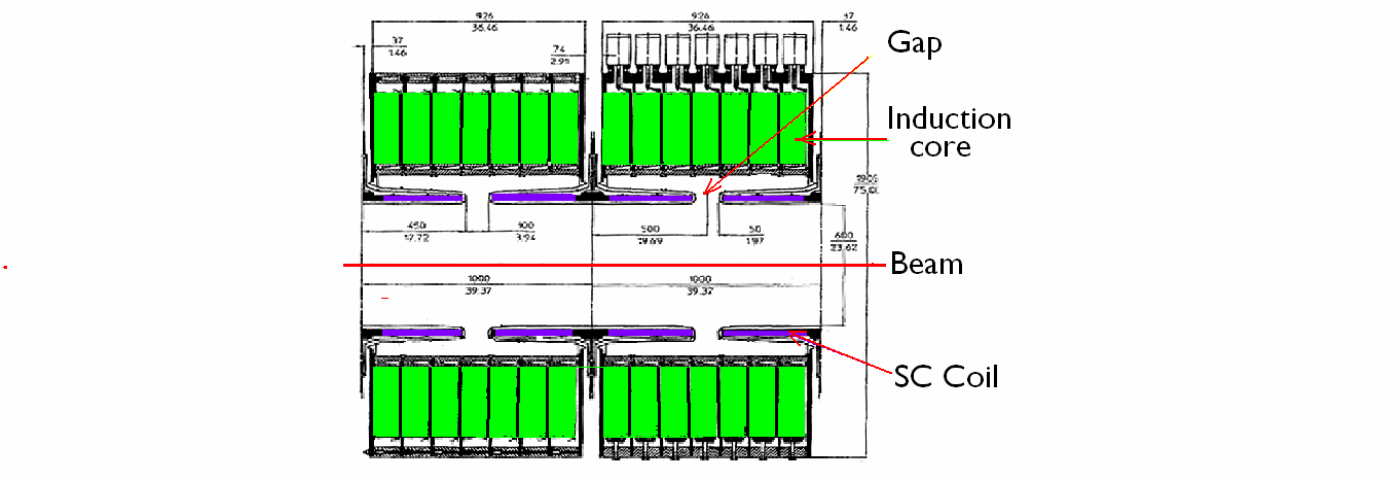

Figure 8: Induction unit design taken from Feasibility Study II for a Neutrino Factory.

Successful demonstration of phase rotation and re-acceleration between solenoid stages

The optimization varied the rf frequency, phase, lengths and locations of the induction acceleration units so as to:

a) Accelerate the muons to the input energy for the next cooling stage;
b) Use drifting to allow the bunch length to rise to the value needed for the next stage; and
c) Phase rotate the bunch to reduce the momentum spread as required.

Towards the end of the 50 T cooling stages shown in Figure 5, the bunches are very long (5 m) and the rf to accelerate and phase rotate the bunches must have a low frequency (1 MHz). To reduce this loss, it was decided to cool using a somewhat higher muon energy that, for the same specified longitudinal emittance (72 pi mm), required bunches of approximately 2 m rms length and rf frequencies of the order of 5 MHz. In fact we did use simple sinusoidal wave forms, as in a conventional rf cavity. But since only a fraction of a cycle of the rf is used (see Figure 9), it is appropriate to use pulsed Induction Linacs, rather than rf cavities. The required pulse lengths were of the order of 60 nsec. It was assumed that these induction units would be similar to those specified for phase rotation in the Study 2 for a Neutrino Factory [ref 20]. Such units could give gradients up to approximately 1 MV/m, as specified here. The wave forms used are shown in Figure 9. The positions and lengths of the linacs are shown in Table 2, the phases being defined relative to a reference particle starting at the center of the injected muon bunch, and propagating forward with a constant momentum of 54 MeV/c.

Table 2: Dimensions and current densities of coils forming 50 T solenoid, matching in and out, and in Induction Linac beam transport.

50 T Solenoid and Matching

	len1 m	gap m	dl m	rad m	dr m	I/A A/mm^2
1	0.000	0.000	1.000	0.100	0.020	50.00
2	1.000	0.000	1.000	0.100	0.020	50.00
3	2.000	0.000	1.000	0.100	0.020	50.00
4	3.000	0.000	0.200	0.100	0.020	50.00
5	3.200	0.000	0.200	0.100	0.020	49.75
6	3.400	0.000	0.200	0.100	0.020	49.50
7	3.600	0.000	0.200	0.100	0.020	49.25
8	3.800	0.000	0.200	0.100	0.020	49.00
9	4.000	0.000	0.200	0.100	0.020	48.75
10	4.200	0.000	0.200	0.100	0.020	48.50
11	4.400	0.000	0.200	0.100	0.020	48.25
12	4.600	0.000	0.200	0.100	0.020	48.00
13	4.800	0.000	0.200	0.100	0.020	47.75
14	5.000	0.000	0.200	0.100	0.020	47.50
15	5.200	0.000	0.200	0.100	0.020	47.25
16	5.400	0.000	0.200	0.100	0.020	47.00
17	5.600	0.000	0.200	0.100	0.020	46.75
18	5.800	0.000	0.200	0.100	0.020	46.50
19	6.000	0.000	0.200	0.100	0.020	46.25
20	6.200	0.000	0.200	0.100	0.020	45.00
21	6.400	0.000	0.200	0.100	0.020	40.00
22	6.600	0.000	0.200	0.100	0.020	35.00
23	6.800	0.000	0.200	0.100	0.020	27.50
24	7.000	0.000	0.200	0.100	0.020	20.00
25	7.200	0.000	0.200	0.100	0.020	12.50
27	7.842	-.158	0.317	0.025	0.029	164.26
28	7.832	-.327	0.337	0.055	0.041	142.43
29	7.812	-.356	0.375	0.098	0.056	125.88
30	7.783	-.404	0.433	0.157	0.067	119.07
31	7.748	-.468	0.503	0.228	0.120	85.99
32	7.565	-.686	0.869	0.355	0.089	39.60
33	7.566	-.868	0.868	0.454	0.104	44.30
34	7.504	-.930	0.992	0.575	0.252	38.60
36	8.600	0.104	0.200	0.100	0.020	12.50
37	8.800	0.000	0.200	0.100	0.020	20.00

50 T Solenoid and Matching (contin)

	len1 m	gap m	dl m	rad m	dr m	I/A A/mm^2
38	9.000	0.000	0.200	0.100	0.020	27.50
39	9.200	0.000	0.200	0.100	0.020	35.00
40	9.400	0.000	0.200	0.100	0.020	40.00
41	9.600	0.000	0.200	0.100	0.020	45.00
42	9.800	0.000	0.200	0.100	0.020	46.25
43	10.000	0.000	0.200	0.100	0.020	46.50
44	10.200	0.000	0.200	0.100	0.020	46.75
45	10.400	0.000	0.200	0.100	0.020	47.00
46	10.600	0.000	0.200	0.100	0.020	47.25
47	10.800	0.000	0.200	0.100	0.020	47.50
48	11.000	0.000	0.200	0.100	0.020	47.75
49	11.200	0.000	0.200	0.100	0.020	48.00
50	11.400	0.000	0.200	0.100	0.020	48.25
51	11.600	0.000	0.200	0.100	0.020	48.50
52	11.800	0.000	0.200	0.100	0.020	48.75
53	12.000	0.000	0.200	0.100	0.020	49.00
54	12.200	0.000	0.200	0.100	0.020	49.25
55	12.400	0.000	0.200	0.100	0.020	49.50
56	12.600	0.000	0.200	0.100	0.020	49.75
57	12.800	0.000	0.200	0.100	0.020	50.00
58	13.000	0.000	1.000	0.100	0.020	50.00
59	14.000	0.000	1.000	0.100	0.020	50.00

Transport in Induction Unit

	len1 m	gap m	dl m	rad m	dr m	I/A A/mm^2
60	15.000	0.000	1.000	0.100	0.020	50.00
61	16.000	0.000	1.000	0.100	0.020	50.00
62	17.000	0.000	1.000	0.100	0.020	50.00
63	18.000	0.000	1.000	0.100	0.020	50.00
64	19.000	0.000	1.000	0.100	0.020	50.00
65	20.000	0.000	1.000	0.100	0.020	50.00
66	21.000	0.000	1.000	0.100	0.020	50.00
67	22.000	0.000	1.000	0.100	0.020	50.00

Table 3: Lengths and Positions of Induction Accelerators.

Waveform in Figure 9		a)	b)
Distance from previous magnet center (m)		6.1	11.1
Length	(m)	5	1
Frequency	(MHz)	5	15
Phase	(deg)	65	110
Gradient amplitude	(MV/m)	0.64	0.6

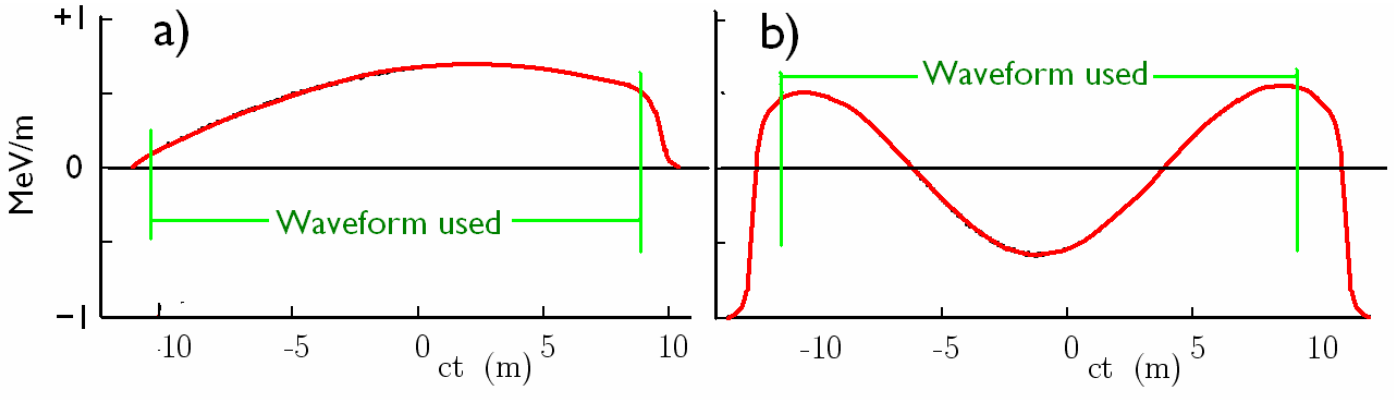

Figure 9: Wave forms used in the phase rotation and acceleration: a) is used in initial 5 m and b) in final 1 m.

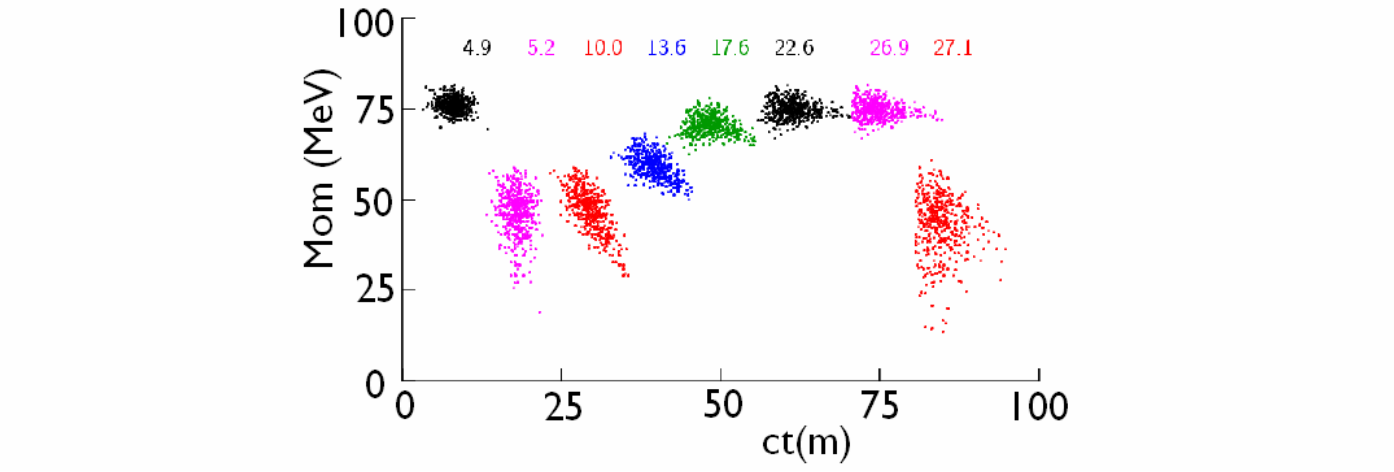

Figure 10: Longitudinal momenta vs. time at specified distances (m) along the system. The horizontal positions of individual distributions have been arbitrarily shifted to separate their distributions.

Figure 10 shows the longitudinal phase spaces at a sequence of locations along the system. The distribution at 4.9 m represents the phase space entering the first hydrogen absorber. At 5.2 m, after the absorber, the energy has dropped and the energy spread increased by straggling and the negative value of the slope of dE/dx with the energy E. The distributions at 10.0 – 17.6 m show the progressive phase rotation and acceleration. Between 17.6 and 22.6 m the final induction units use a higher frequency section that helps straighten the distribution. The distributions at 26.9 and 27.1 m show the energy loss in the second hydrogen absorber.

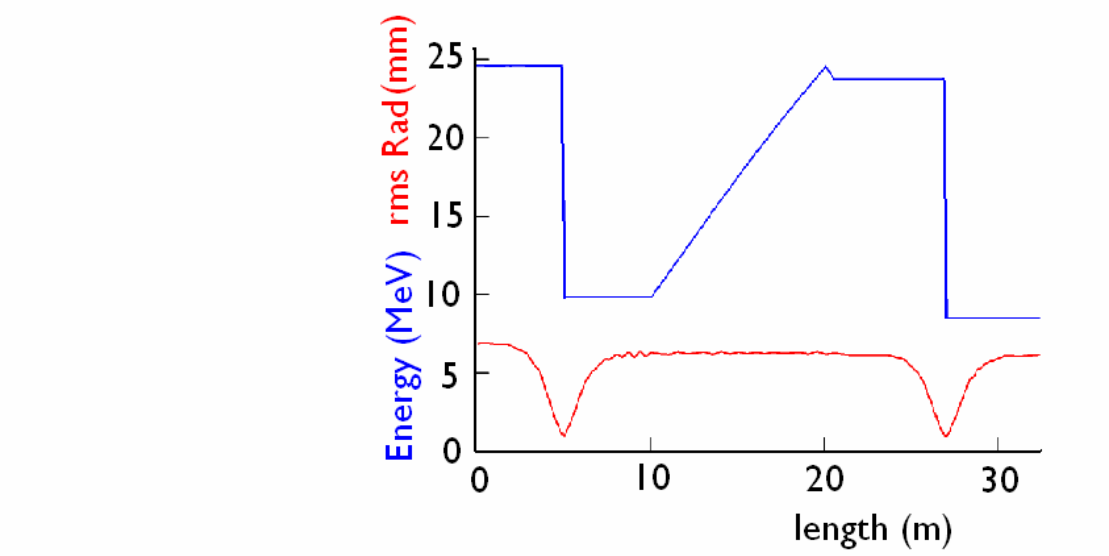

Figure 11: Average Energy and rms bunch diameters vs. length.

Figure 11 shows the ICOOL simulated rms beam sizes through the system. It is seen that it is approximately 1 mm in the 50 T solenoids, allowing the liquid hydrogen pipe inside the magnets to have a diameter of 1-2 cm. Both hydrogen absorbers in this simulation had lengths of 18 cm, and they were centered in the 50 T magnets. The liquid would be circulated to remove the heat from the beam ionization. The beam diameter in the transport solenoids is still only about 6.5 mm, allowing a 6-8 cm diameter pipe.

Figure 12a shows the simulated emittances vs. length showing the drop in transverse emittance and rises in longitudinal emittance in the hydrogen inside the two 50 T solenoids. It is seen that both emittances remain essentially constant during the matching, phase rotation and re-acceleration. The only significant dilution is in the longitudinal emittance that rises approximately 2%. The muon loss was 12.5% with 5% of this from decay and the rest (7.5%) from the loss of muons in the Landau tails after each hydrogen absorber that are lost by their stopping in the absorber, or beyond the 4 sigma cut employed in defining the plotted emittances.

Figure 12b shows the transverse emittances plotted against the longitudinal emittances, again showing the transverse emittance falling, as the longitudinal emittance rises, and the very small changes in either in the matching, transport and re-acceleration.

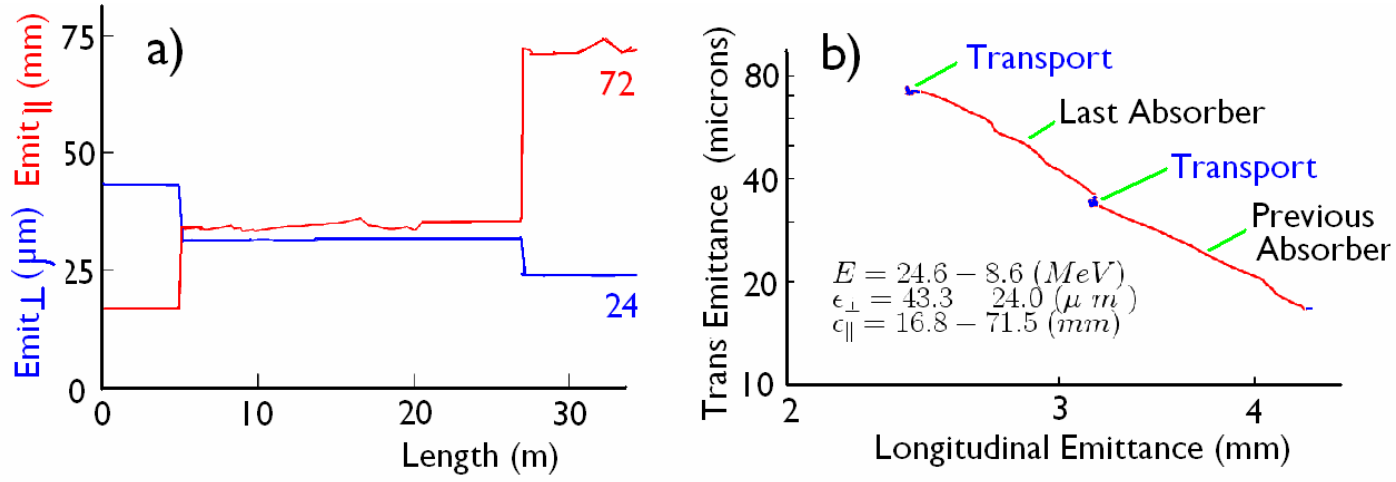

Figure 12: a) Transverse and longitudinal emittance vs. length; b) Transverse vs. longitudinal emittance through the two cooling stages.

b) Study of 50 T Magnet Design Feasibility, Power Consumption & Superconductor Cost

Extrapolation of NHMFL 45 T hybrid magnet to 50 T

A proof-of-principle magnet at a field strength only 10% shy of 50 T is the 45 T NHMFL hybrid magnet of Figure 2. Its design parameters are 14 T from a superconducting (SC) magnet and 31 T from a resistive insert using 24 MW. Several years ago the insert was upgraded to 34 T at 29 MW to regain the 3 T lost when the innermost superconducting coil was damaged by an unprotected quench. With a superconducting magnet of 14 T the field with 29 MW should be more than 47 T—though less than 14+34 = 48 T, because the higher field requires conductors that are stronger, and hence more resistive.

To reach 50 T with a superconducting magnet identical to that of the NHMFL 45 T system requires a further upgrade of the insert. Extrapolation suggests that 36 T from the insert magnet should be possible using ~34 MW. Provided that one can obtain satisfactory magnet longevity despite the higher operating temperature, the technical feasibility of a 50 T magnet is not much in doubt.

Superconductor current density J_e vs. ambient field B

However, such a magnet would be very expensive to run. Assuming electricity at 10¢/kW-hr, 34 MW times 8,766 hours/year is $30 million a year! Economics dictates that the superconducting coils contribute as much as feasible to the field. Magnets employing Nb_3Sn cooled to < 2 K by superfluid helium have demonstrated their ability to reach fields at least 21.2 T (900 MHz MRI). Figure 13 shows that Bi-2212 and Bi-2223 carry respectable current to fields that are much higher still.

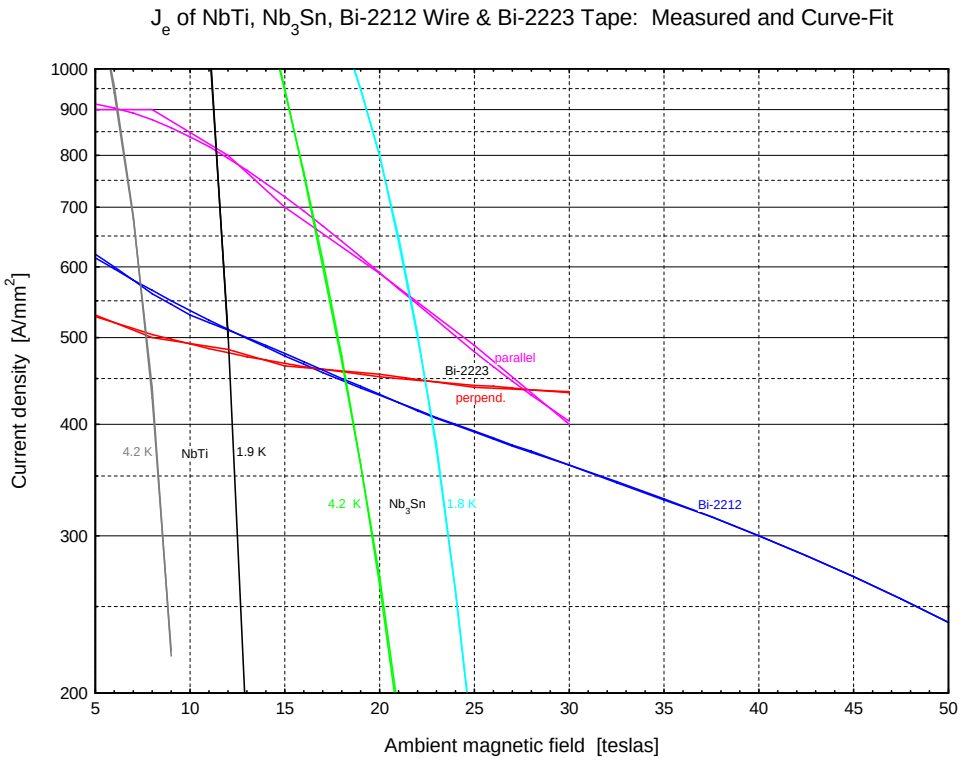

Figure 13: $J_e(B)$ for NbTi, Nb_3Sn and Bi-2212 wire, as compiled by Peter Lee, and for Bi-2223 tape, by Yukikazu Iwasa. Smooth curves fit the raw data by $\log_{10}(J_e) = c_0 + c_1B + c_2B^2 + c_3B^3$.

The current densities in Figure 13 are "engineering" current densities (hence the subscript on J_e), i.e., averaged over the entire conductor, including any matrix or non-matrix metal inherent in its manufacture. For Bi-2212 this percentage presently is high: 72%. Wire manufacturers must find a way to lower this percentage if Bi-2212 is to achieve the overall current densities called for in the designs below despite the sizeable fraction of winding cross section that must be allocated to structural reinforcement or is unavoidably lost to "voids" for insulation, impregnant, and perhaps coolant.

Design philosophy

Figure 14a sketches the windings cross sections of the superconducting and resistive coils of a 50 T hybrid magnet system with SC coils identical to those in the NHMFL 45 T magnet. The resistive coils are Bitter coils, as invented by M.I.T. professor Francis Bitter and improved by the Francis Bitter National Magnet Laboratory and National High Magnetic Field Laboratory. Phase I explored the replacement of some or all of the Bitter coils with superconducting coils in order to reduce the power consumption. Figure 14b sketches the geometry after replacement of the outermost Bitter coil.

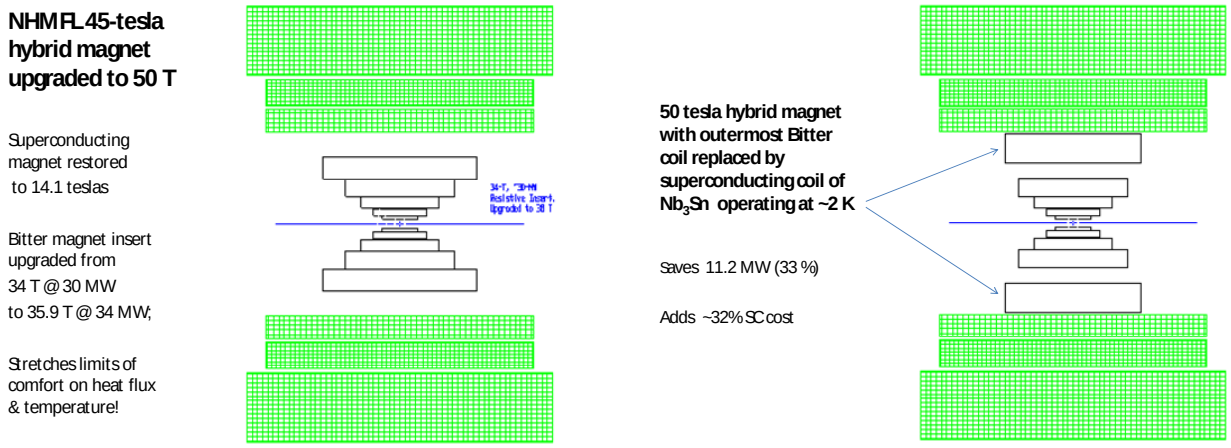

Figure 14: a) NHMFL 45 T hybrid magnet upgraded to 50 T with Bitter insert of 36 T @ 34 MW. b) 50 T hybrid magnet, with SC coils identical to those in Figure 14a, with the outermost Bitter coil replaced with a SC coil of Nb_3Sn at 2 K, saving 11.2 MW at the price of an additional 32% in material.

Compared to the Bitter coil that it replaces, the innermost superconducting coil is bigger by a ratio of 4:3 in both inner and outer diameter. That the O.D. can be larger is because the superconducting coil can appropriate space previously preempted for the magnet housing for the Bitter magnet and the bore tubes and vacuum spaces of the cryostat for the superconducting coils. That the radial gap between the innermost superconducting coil and the outermost Bitter coil is less in Figure 14b than it was in Figure 14a is because thinner tubes and vacuum gaps suffice for the smaller bore tube and Bitter magnet housing.

Replacing the outermost Bitter magnet is the logical place to start because (1) it consumes the most power, and (2) the maximum field point approximates the 21.2 T proved feasible in 900 MHz NMR magnets at sub-lambda temperature. Figure 13 shows that even at this high field internal-tin process Nb_3Sn has a J_e of approximately 600 A/mm^2, which is adequate for solenoids [ref. 21]. Since this field range is within reach for Nb_3Sn, it is the obvious choice, due to its much lower cost than HTS [ref. 22].

Replacing further Bitter solenoids with superconducting coils

The obvious approach to design a sequence of hybrid magnets with an arbitrary number of substitutions of superconducting coils for Bitter coils is to sequentially replace each successive Bitter coil, working inwards from the outermost coil. However, such a technique could encounter a bottleneck if any Bitter coil was of such high performance as to be beyond the capacity of any superconducting coil to replace it. Therefore we have adopted a complementary approach. We first designed an all-superconducting magnet in which all coils were of comparable technological difficulty, as measured by the criterion—admittedly somewhat arbitrary—of equal percentage of matrix metal, an approximate indicator of the difficulty of quench protection. The magnet required optimistic assumptions, to be discussed later, on materials and methods for magnet reinforcement and quench protection, thereby suggesting topics for fruitful superconducting wire research and development.

The resulting base design has superconducting coils with parameters that remain unchanged as, at

each stage, one sequentially replaces its innermost coil with a Bitter coil and re-optimizes the Bitter magnet to minimize its power consumption. Figure 15 sketches the coil conductor cross sections at each stage of the process. Each Bitter coil is ¾ the I.D. and O.D. of the superconducting coil that it replaces because the design has shifted from inside to outside the Bitter magnet housing and cryostat walls and vacuum spaces. The savings in SC cost and attendant penalty in Bitter-magnet power consumption give the trade-off of superconductor materials cost and Bitter magnet power.

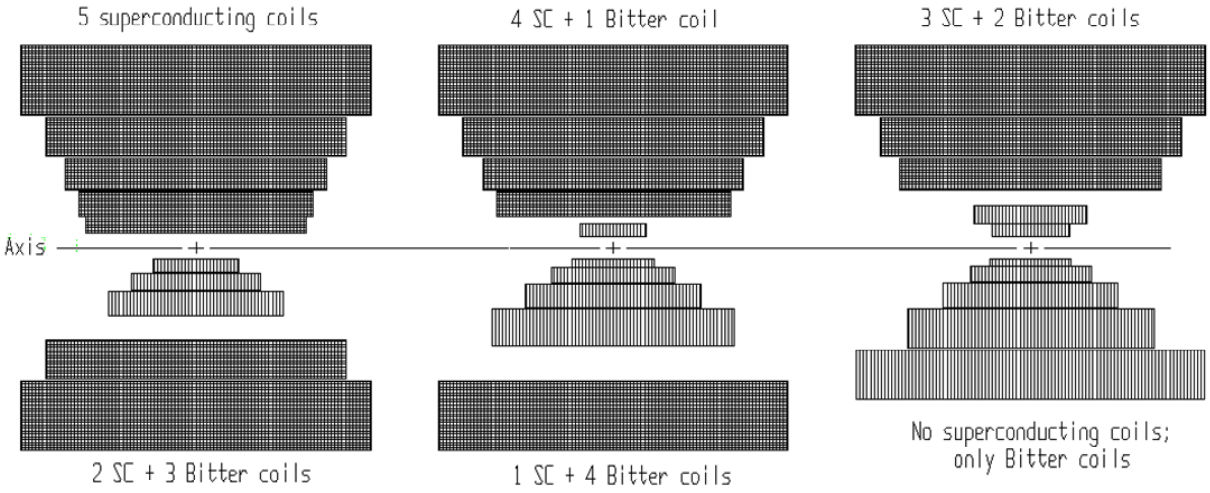

Figure 15: Windings cross section of innermost five coils of sequence of six hybrid magnets. The base design is at top left; design #5 at bottom right has only Bitter coils.

Estimation of coil volume devoted to voids, superconductor, reinforcement and matrix

The design of each magnet system of course requires iteration. The first step is to assume a set of candidate coil dimensions and overall current densities, j_{coil}. One then calculates the magnetic field throughout each coil, as in Figure 16a. This enables one to estimate the stresses throughout each coil, and to determine the maximum ambient field seen by each superconducting coil, as in Figure 16b.

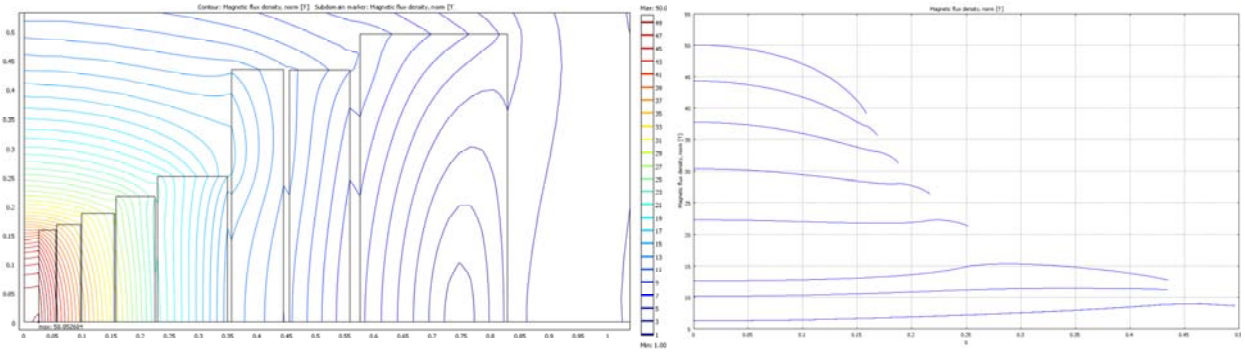

Figure 16: a) Field magnitude inside and in vicinity of coils of all-superconducting 50 T magnet. b) Field magnitude along inner radius of each coil, from magnet midplane to each coil end. The maximum field, in teslas, in each of the consecutive coils, from outermost to innermost, is 9.0, 11.3, 15.4, 22.4, 30.4, 37.8, 44.2 & 50.1, respectively.

For superconductors which are sensitive only to field magnitude, not field orientation, Figure 16b, in conjunction with Figure 13, determines the current density which the superconductor in that coil can support. In order to simplify computations Phase I elected not to consider Bi-2223 and YBCO, because of their sensitivity to field orientation. Phase II proposes to consider these conductors.

The needed fractional volume of superconductor, f_{SC}, is j_{coil} / j_e. From the coil current densities and ambient magnetic field distribution one can compute the average (or peak) stress σ_{coil} in each coil. The fraction of coil volume needed for mechanical support then is $f_{support} = [\sigma_{coil} - f_{SC}*\sigma_{SC} - (1 - f_{void} - f_{SC}) * \sigma_{matrix}] / (\sigma_{support} - \sigma_{matrix})$, where σ_{SC} is the stress that the superconductor can withstand without significant degradation. The fractional volume of matrix f_{matrix} is what remains: $f_{matrix} = 1 - f_{SC} - f_{support} - f_{void}$. The volume of superconductor, reinforcement material and matrix metal in each coil, times the unit cost for each, determine the total material cost.

Unit cost of superconductor, matrix, and reinforcement

The cost per unit volume of each superconductor is derived from [ref 26]: Nb_3Sn (12T, 4.2K, 50% Cu stabilizer) = \$5.50/kA-m; \$1000/kg; and Bi-2212 (20T, 4.2K, 75% Ag matrix) = \$64/kA-m; \$3,470/kg. The cost per cubic centimeter of winding of each coil is the sum of that for the superconductor itself, matrix metal, and additional reinforcement material, if any. The unit cost of each superconductor one can deduce as the product of the current density in Figure 13 (in kA/mm^2) and the cost in \$/kA-m: $\$/cm^3 = (\$/kA\text{-}m) * (kA/mm^2) * (1\ m\text{-}mm^2/cm^3)$.

For NbTi a cost of \$1/kA-m @ (5T, 4.2K), multiplied by the 5-T current density of 1.23 kA/mm^2, translates to $\$1.23/cm^3$. \$5.50/kA-m for Nb_3Sn @ (12T, 4.2K), multiplied by the 12-T current density of 1.724 kA/mm^2, translates to $\$9.48/cm^3$. \$64/kA-m for Bi-2212 @ (20T, 4.2K), multiplied by the 20-T current density of 0.431/0.28 = 1.539 kA/mm^2, translates to $\$98.52/cm^3$. The analyses to follow estimate the cost of copper matrix metal to be $\$1/cm^3$, and that of structural reinforcement to be $\$1/cm^3$ if of stainless steel, and $\$10/cm^3$ if of tungsten. For any coil of Bi-2212 or Nb_3Sn with a high fraction of superconductor a very crude estimate for these costs suffices, because the superconductor cost is so preponderant.

Design #0: All-Superconducting Magnet

The above equations permit the estimation of material costs for any superconducting magnet. The computer program that incorporates these equations solves iteratively for the parameters that satisfy all constraints on field and stress and equalizes the matrix fraction in the inner five coils. It also minimizes the cost of materials—superconductor, matrix and reinforcement. Figure 17a graphs how the cost increases with increasing fraction of matrix metal in order to facilitate quench protection. Cost minimization of a magnet with all-superconducting coils using these input parameters, and a matrix fraction of 38.5% in all five insert coils, leads to a winding cross section as sketched in "Design #0: All-SC coils", the upper-leftmost of the six half-coil sets of Figure 15. Figure 17b tabulates various parameters for this magnet.

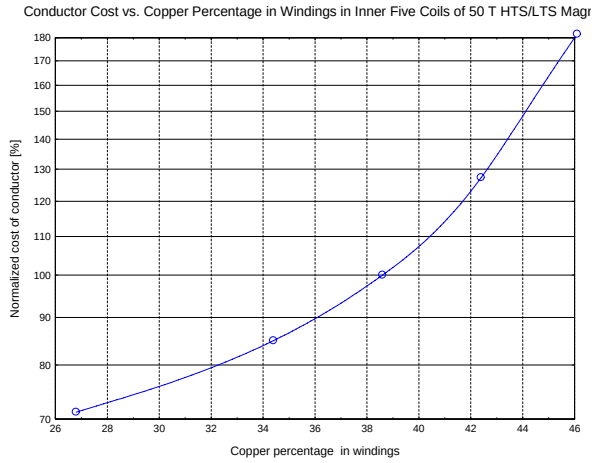

Parameters of 50-Tesla All-Superconducting Magnet

Coil	B_{max}	jλ	σ_{avg}	Void	SC	Reinf.	Matrix	Cost
	T	A/mm^2	MPa	%	%	%	%	M$
NbTi	9.0	38.6	max.=139	40	1.9	11.5	46.6	0.67
Outer Nb_3Sn	11.2	44.3	203	40	2.7	23.6	33.7	0.24
Inner Nb_3Sn	14.8	39.6	190	40	5.1	21.2	33.7	0.20
2K Nb_3Sn	22.3	86.0	426	20	23.7	17.8	38.6	0.48
BSCCO #1	30.3	119	594	20	14.7	26.7	38.6	0.61
BSCCO #2	37.7	126	538	20	17.8	23.7	38.5	0.34
BSCCO #3	44.3	142	441	20	23.0	18.6	38.4	0.16
BSCCO #4	50.0	164	306	20	30.3	11.3	38.4	0.072

Figure 17: a) Material cost vs. matrix fraction for five-coil insert of 50-T all-superconducting magnet. b) Parameters of 50-T all-superconducting magnet with 38.5% matrix in inner five coils.

Trade-off of Superconducting Magnet Cost and Bitter Magnet Power

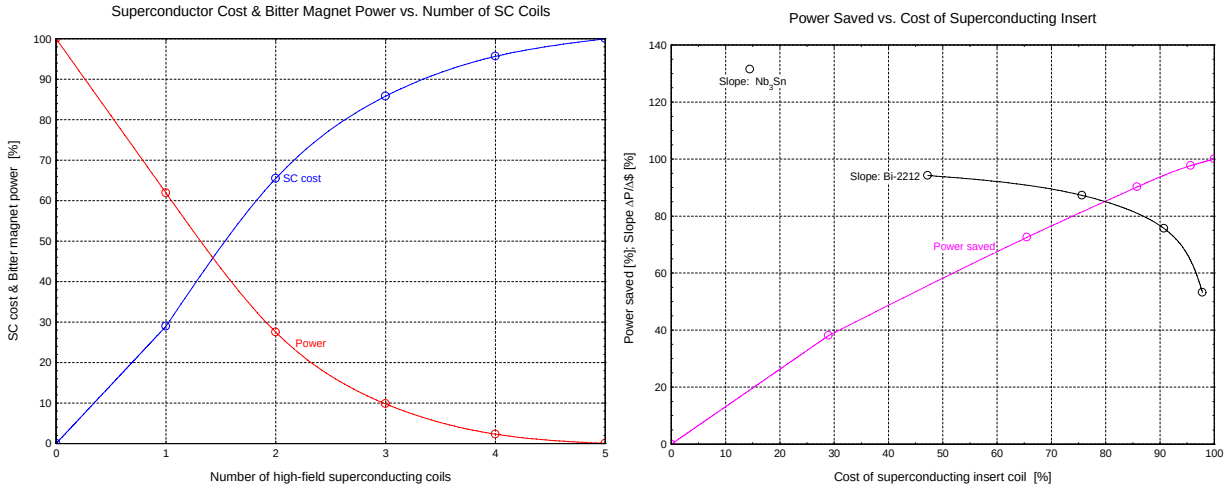

Figure 18: a) Normalized materials cost and power consumption of 50 T hybrid magnets with inserts with zero to five SC coils. b) Trade-off of materials cost vs. Bitter magnet power consumption.

Figure 18a graphs the normalized magnet materials cost and power for insert magnets with from zero to five superconducting coils—Designs #0 through #5. One endpoint, Design #5, employs a 34 MW, 36 T insert to upgrade the NHMFL hybrid to 50 T. The other endpoint, Design #0, is an all-superconducting magnet costing about one and a half times as much as the 14 T superconducting magnet of the NHMFL hybrid. Note that the first SC-for-Bitter substitution, with a Nb_3Sn coil operating at 2 K, reduces the power consumption of the hybrid magnet by 38% with an increase in cost of only 29% that of the entire five-coil superconducting insert.

Graphing the power saved (red curve of Figure 18a) vs. the materials cost invested (blue curve) yields the magenta curve of Figure 18b. Evaluating the secant slopes between adjacent data points yields the black curve. The curves confirm one's intuition that replacing Bitter coils with

superconducting coils becomes gradually less and less rewarding. The first substitution is by far the most productive, with a slope of 132%. The fruitfulness of this substitution is much higher than for any subsequent one because the superconducting coil is of Nb_3Sn, whose unit cost is so much less than Bi-2212. Replacement of Bitter coils with Bi-2212 coils is substantially less rewarding. Secant slopes of the successive substitutions diminish at an ever-increasing rate: 94%, 87%, 76% and 53%.

Nonetheless, the economic incentive for Bitter-to-SC substitution remains economically compelling all the way through to the all-superconducting endpoint. Replacing the last Bitter coil costs ~$72K to save "only" 0.78 MW. Even this comparatively "modest" power consumption, however, costs about $700 K a year, enough to justify an additional investment of ~$7M beyond the approximately $300M justified by the rest of the Bitter-to-SC magnet substitutions.

More accurate stress analyses

Because all five coils of the insert have high current densities and are exposed to high ambient fields, stresses are high, requiring substantial reinforcement. Figure 19a plots the hoop stress that the coil windings of all eight coils would experience if turns did not interact via radial tension or compression. Figure 19b plots the hoop stress in bonded coils. Compared to Figure 19a, the maximum hoop stress in the outermost coil is less, because outer layers of windings support inner layers via radial compression. In all other coils, however, the maximum hoop stress is much worse, because outer layers tug radially on inner layers via radial tension.

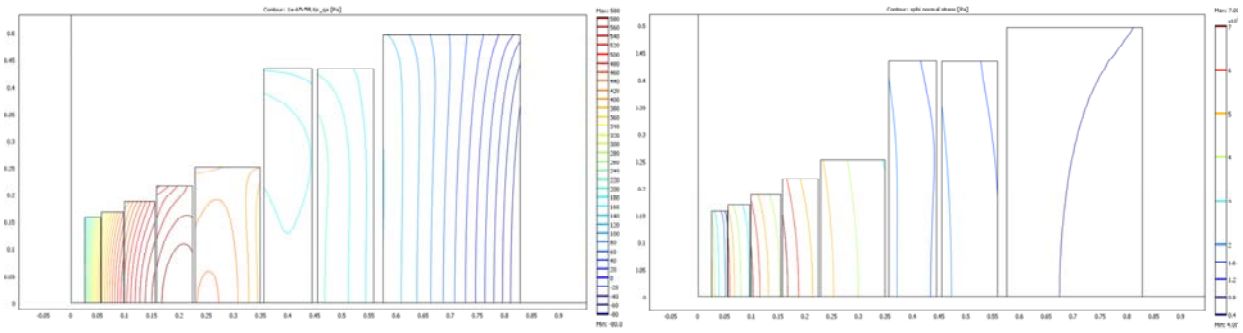

Figure 19: a) Hoop stress in absence of radial-load transmission. Maximum stress, in MPa, in consecutive coils, from innermost to outermost, is 394, 516, 586, 599, 443, 198, 208 & 141, respectively. b) Hoop stress in bonded magnet with no winding pretension. Maximum stress in consecutive coils is much higher: 509, 644, 733, 756, 569, 212, 210 & 65 MPa, respectively.

One way to alleviate the aggravation of hoop stress caused by radial tension is to overwrap each coil with banding of a material that is very strong and, ideally, stiff as well. However, this works well only for coils that are radially relatively thin so that the effect of the banding can propagate all the way to the inner radius. More versatile is to wind the conductor under tension. Figure 20a plots contours of hoop stress with winding tensions in consecutive coils chosen to minimize the maximum hoop stress in each coil. Figure 20b plots contours of radial stress with winding pretension as in Figure 20a. Except for the inner two coils, the radial stress is either compressive (OK, if not extremely large) or only slightly tensile. The inner two coils may require radial partitioning to reduce the radial tension which might cause the coils to delaminate.

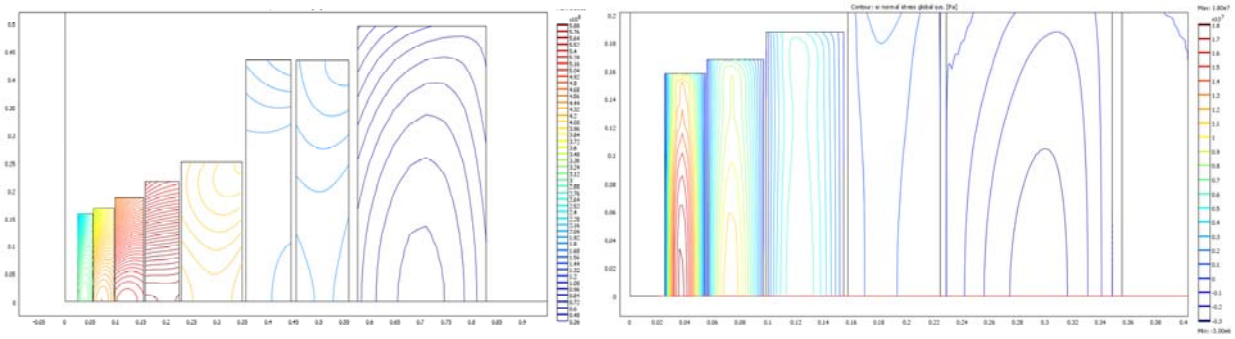

Figure 20: a) Hoop stress with winding pretensions, in MPa, in consecutive coils of 291, 422, 505, 547, 396, 165, 162 & 40, respectively. Compared to Figure 19b, the maximum stress is much reduced: 308, 442, 535, 588, 422, 182, 183 & 56 MPa, respectively. b) Radial stress in innermost five coils with winding pretension as at left. The inner two coils may need radial partitioning to reduce the radial tension which might cause delamination.

Consideration of YBCO conductor

As an alternative to Bi-2212, some of the highest field (smallest) solenoids perhaps can be wound with YBCO. YBCO has a very high J_c at high fields, although this advantage is somewhat reduced in practice by three factors. First, the J_e is greatly reduced due to the substrate and buffer layers that must be incorporated into a practical conductor. Second, YBCO J_c values are highly anisotropic. Third, in contrast to Nb_3Sn and Bi-2212 that are available as round wires, YBCO is available only as a high aspect ratio tape, and is more challenging to use in a practical coil.

Nevertheless, Figure 21a reveals that YBCO has a current density much superior to Bi-2212 provided that the field orientation is sufficiently favorable so that the appropriate curve is more like that for a parallel field rather than a perpendicular one. Figure 21b shows that the maximum field angle is about 8° for the innermost coil, 12° for the second coil, and 17° for the third coil.

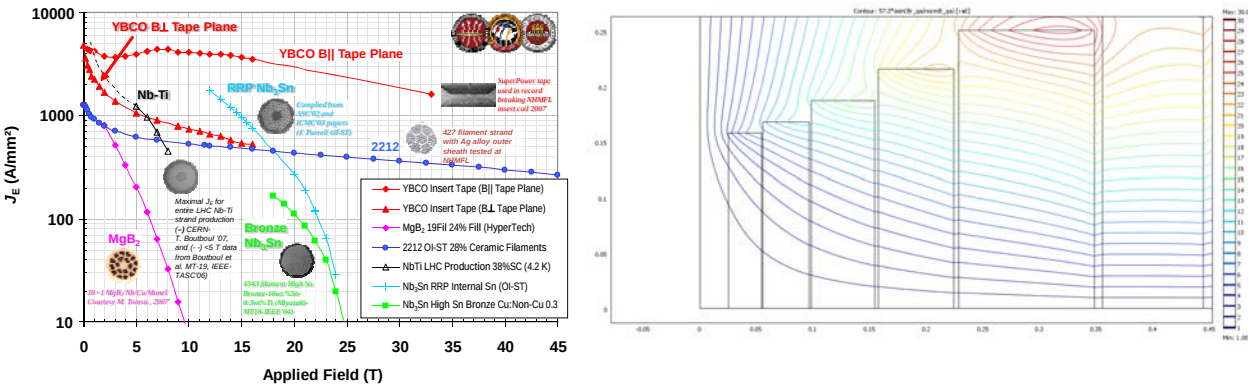

Figure 21: a) Engineering current density of YBCO, demonstrating its potential superiority over Bi-2212. b) Contours of field orientation in 50-T all-superconducting magnet, demonstrating that the field orientation in the innermost coils may be sufficiently favorable for YBCO.

Comments & caveats on the trade-off of SC magnet cost and Bitter magnet power

In this preliminary analysis of the trade-off between the cost of resistive coils and the cost to replace them with superconducting coils, only the cost of the superconducting materials, stabilizing materials, and structure were included in the cost estimate for superconducting coils; i.e., construction costs were not included. While construction costs are significant, they are very design dependent and will be left as a Phase II task. Phase II proposes to construct small insert coils of Bi-2212 and YBCO; this work will generate some coil construction cost information. Likewise, for the resistive magnets the construction costs and materials costs were not considered, but only the operating power costs. The cost of power for this comparison was \$0.10/kW-hr. Upgrading the NHMFL hybrid to 50 T (keeping all resistive coils) was projected to need 34 MW, for a yearly operating cost of \$30M. The intent was to examine the major cost factor for each system (materials for the superconducting coils, and power for the resistive coils) in order to evaluate the impact of replacing one or more of the resistive coils.

At fields above about 22 T, Bi-2212 has a J_e superior to that for Nb_3Sn. It is important to work with J_e rather than J_c for Bi-2212, since the manufacturing process requires that a minimum Ag-matrix-to-superconductor-volume of 3:1 be maintained. Taking this into account, the current density J_e of ~240 A/mm^2 at 50 T, and even the ~360 A/mm^2 at 30 T, is inadequate for the designs here, given the volume fraction needed for reinforcement, insulation and impregnant. To become truly feasible, a highly-stressed magnet using Bi-2212 needs research and development to improve the manufacture of the superconductor.

A major issue with using Bi-2212 for these solenoids is that the strain tolerance of Bi-2212 superconducting wire is not well known, especially at high fields. With Nb_3Sn, and possibly for YBCO as well, the magnet designer can apply compressive pre-strain to the conductors to keep the superconductor in a safe strain range. This can be done by banding, for example. With Bi-2212, it is not clear that this approach can be used, since some early results indicated that the Bi-2212 showed a permanent J_c degradation in transverse compression. However, modern Bi-2212 wires are greatly improved over earlier versions, so concern over compressive stress may not be warranted anymore. This is an area calling for continued R&D.

Another major issue is how to react the Bi-2212 material. The reaction procedure used at present is very demanding, requiring that the temperature be maintained at ±1 C in order to develop the best properties. React-and-wind is of questionable applicability, given the rather large bending strain likely to be incurred during coil winding. Both approaches have been used successfully for winding solenoid inserts at NHMFL [ref 23] and for racetrack coils at LBNL [ref 24] and BNL [ref 25]. However the coils proposed here are larger than the coils referred to above, so it may be more difficult to maintain the exacting reaction temperature range. These key issues are among those to be addressed in a new DOE-funded R&D program devoted to Bi-2212, and funded at \$4M over the next two years. This proposed Phase II program expects to benefit from the results.

Quench protection

The magnetic energy stored by the entire magnet system is very high—about 134 MJ. It is vital to prevent any energy concentration whereby a local region absorbs much more energy than its own. Upon initiation of a quench anywhere, the affected coil must be de-energized rapidly enough to prevent it from overheating. One would like to de-energize most rapidly those coils with the highest

current density. An important discovery of Phase I is that it is indeed possible to do this, if each coil is made to dump its energy into a separate resistor of the correct size. Figure 22 shows that one can reduce the current in all five of the insert coils to half value in as little as one second, while allowing over twenty seconds for the outermost coil to decay to half current. This is a much more comfortable discharge rate for a coil that stores ~70 MJ and hence would generate an unsafe discharge voltage (or else have to run at very high current) were one to discharge it rapidly.

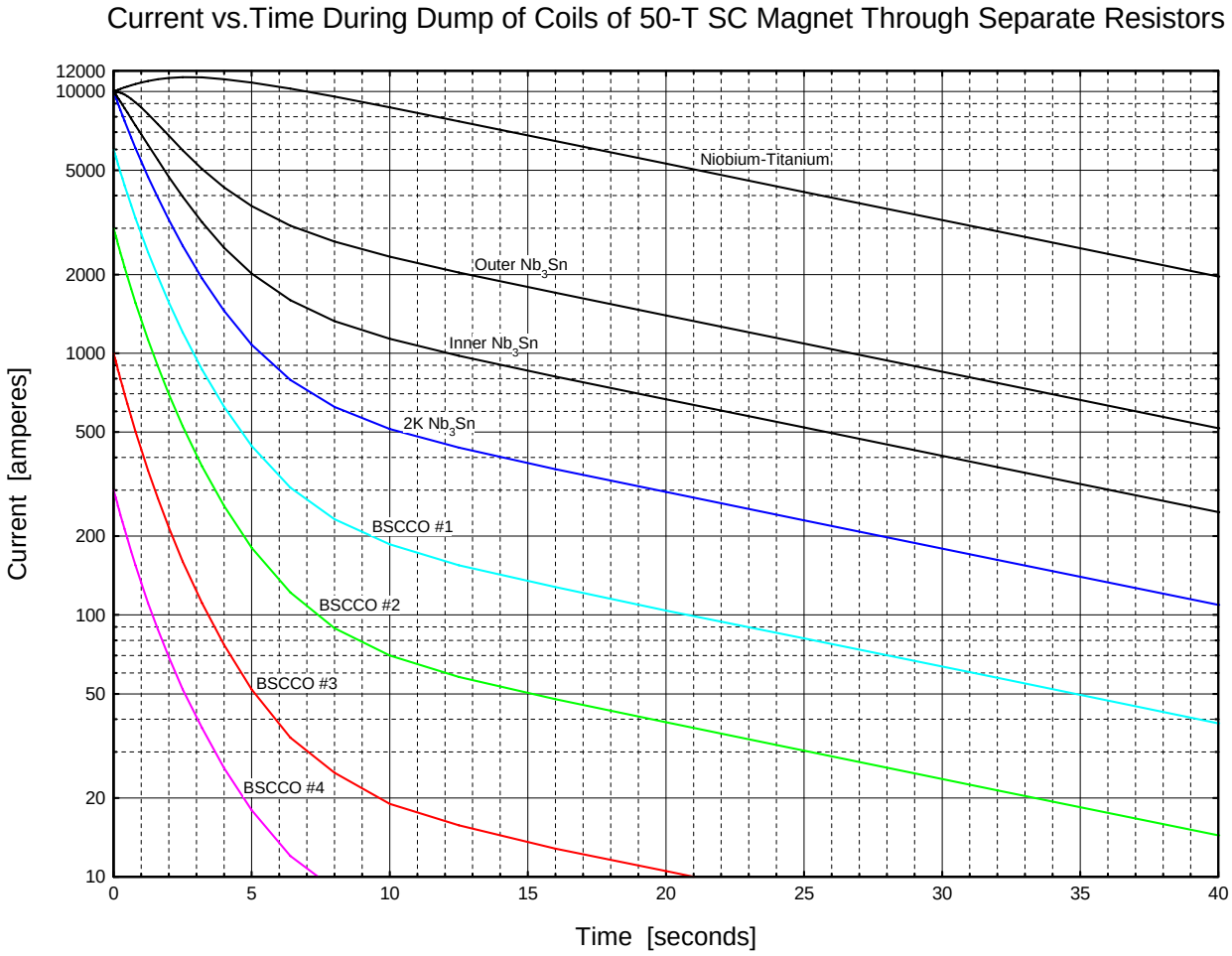

Figure 22: Current vs. time during dump of coils of 50-T all-superconducting magnet through separate resistors.

c) Summary of Phase 1 Achievements

The Phase I technical objectives were:

1) *Find optimized parameters for the sequence of high field solenoid cooling stages, including the required fields, magnet lengths and bore diameters.*

The study concluded that decay losses in the phase rotation and re-acceleration between the later 50 T magnets could be reduced by a) raising the energy in these last stages, and b) increasing the hydrogen lengths to 20 cm.

2) *Consider the implications of these specifications on hybrid 50 T magnet designs that meet these specific requirements.*

We have established that a good field region of 20 cm is adequate for the final 50 T solenoids. Earlier solenoids will be longer.

3) *Do an initial study of the possible power savings that might arise from the use of some HTS materials in the required magnets.*

We have shown that the progressive replacement of resistive coils in a 50 T hybrid design could reduce the power consumption roughly linearly with an increase in superconductor cost.

4) *Determine approximate parameters for the matching and reaccelerating systems between each stage, and simulate cooling through multiple stages using matrix approximations to the matching sections, and simulate the matching from one stage to the next in at least one case.*

We were unable to complete the first part of this task because it was found impossible to achieve satisfactory matching and re-acceleration with a matrix approximation, presumably because of the intrinsic non-linearities involved. But we did achieve the latter more important objective of simulating the matching and re-acceleration, in one case, using adiabatic solenoid matching and sinusoidal rf waveforms. This was an important achievement and gives us reason to believe that the complete system can be designed during the second phase of the study.

III) PROPOSED PHASE II WORK

a) Introduction

The proposed Phase II work is a continuation of a successful Phase I feasibility study and utilizes the 10 T solenoid being developed and built under another PBL, Inc. Phase II effort entitled the "Development of a 6-Dimensional Muon Cooling System Using Achromat Bends and Design, Fabrication and Test of a Prototype High Temperature Superconducting (HTS) Solenoid for the System". This 10 T solenoid will serve as the outer solenoid for the 12 T insert solenoid being proposed herein, thereby leveraging other SBIR funding to achieve even higher field solenoids for muon beam cooling.

In this 2nd phase of the proposal we would continue and expand our study of the use of very high field solenoids for the final muon cooling for muon colliders. The required low emittances can be obtained by passing the muons, at low energies, through liquid hydrogen inside the very high field solenoids. The cooling would be performed in a modest number (7-12) of solenoids, between which the muons would be re-accelerated and phase rotated. The study is innovative because no such optimization of a sequence has yet been performed.

Another innovative approach that would be studied is the bending of the muons between solenoids so that each solenoid is used a number of times, thus reducing their total number, cost and total power consumption.

The 2nd phase would also study the practicality of such very high field solenoids by building a 12 T solenoid that, when tested inside a 10 T HTS solenoid and a 19 T resistive magnet at the NHMFL, would reach a field approaching 40 T.

There would also be expanded work on the design of and optimization of both 50 T and 40 T magnets.

b) Cooling design and simulation

1) Following our achievement, in phase 1, of designing good matching, transport, and re-acceleration between the final two 50 T cooling stages, we will attempt to design similar systems for the earlier stages.
2) Consider parametric changes that could improve the performance of the complete system.
3) Study a cooling sequence using 40 T, instead of 50 T magnets and determine the resulting loss of performance
4) Study the effects of magnet errors on these cooling systems.
5) Study of recirculation of muons through one 50 T cooling stage.

c) Basic hardware used or built

1. Current PBL/BNL [ref 27] ~10 T solenoid (i.d. = 100 mm, o.d. = 165 mm, L ~128 mm)
2. (Proposed BNL) YBCO ~12 T insert (i.d. = 25 mm, o.d. = 95 mm, L ~64 mm)
3. (Proposed Oxford) Bi-2212 ~4 T insert (i.d. = 25 mm, o.d. = 95 mm, L ~64 mm)
4. NHMFL ~19 T resistive solenoid which will provide background field. NHMFL cryostat and test facilities will be used. The dimensions of ~PBL/BNL ~10 T solenoid have been adjusted so that it fits inside. NHMFL cryostat and test facilities will be used.

Each coil is fully self supported (no transfer of radial hoop stress from inner to outer). The construction and testing of both Bi-2212 and YBCO is to learn from the exercise. A real magnet might use Bi-2212 for the magnet ends where the field angles are larger, and YBCO for the inner coils where the field is more parallel.

d) Construction and Testing of ~14-22 T Test "all-HTS" Magnets

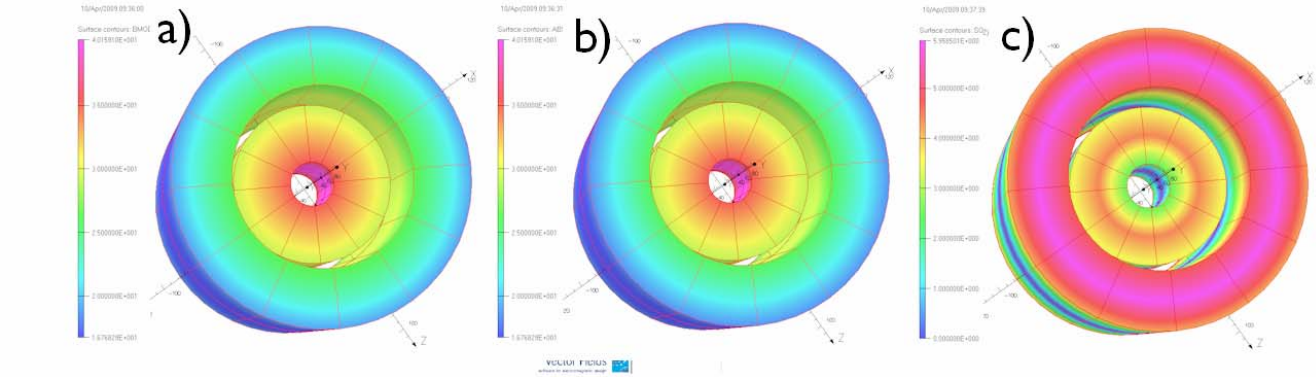

Figure 23: magnetic fields coded by color for the combined 100 mm outer YBCO coils and 25 mm diameter insert YBCO coils; a) of the absolute field magnitudes, b) of the fields in the axial direction (field parallel to the surface of YBCO tape), and c) in the radial direction (field perpendicular to the surface of the tape). Current carrying capacity of the YBCO tape depends on the magnitude and the direction of the field.

BNL will build and individually test 14 YBCO pancakes with 25 mm ID, 95 mm OD. BNL will then build an outer support containing hoop stresses (either wire wrap, or a clamp), and then test all pancakes together giving up to 12 T field. Figure 25 shows the geometry for testing the pancakes of the YBCO insert coil in a vertical dewar at BNL.

Oxford Instruments Superconducting Technology will build a fully reacted Bi-2212 coil with dimensions similar to the YBCO coil built by BNL, but made up of two parts with half their length so that the halves could be used at the ends of the YBCO insert. This coil alone should give approximately 4 T. It will be delivered to BNL for impregnation and instrumentation. It will be tested at 4 K and at higher temperatures.

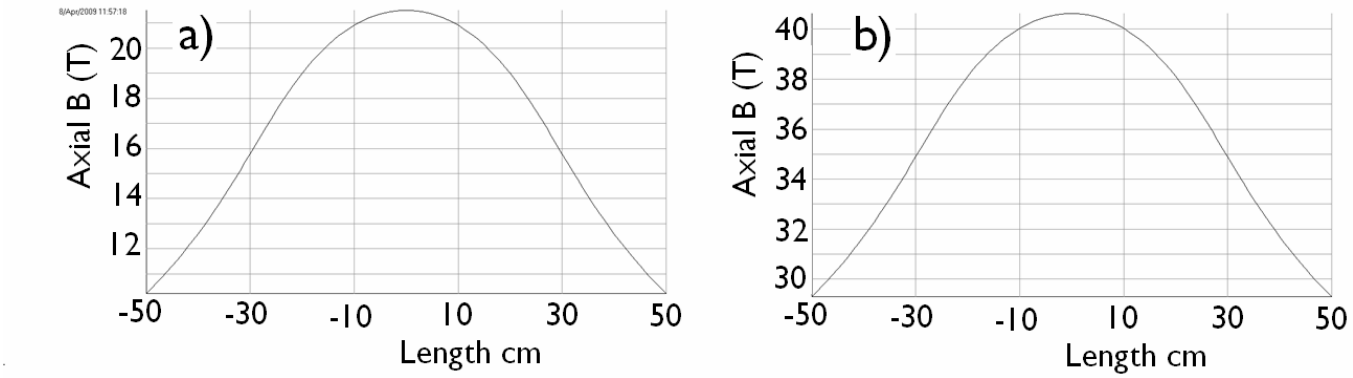

Figure 24: a) Optimistic axial field for combination of YBCO insert and YBCO outsert operating at 4 K; b) Optimistic axial field for combination of YBCO insert and YBCO outsert operating at 4 K; assembled in the NHMFL 19 T resistive magnet.

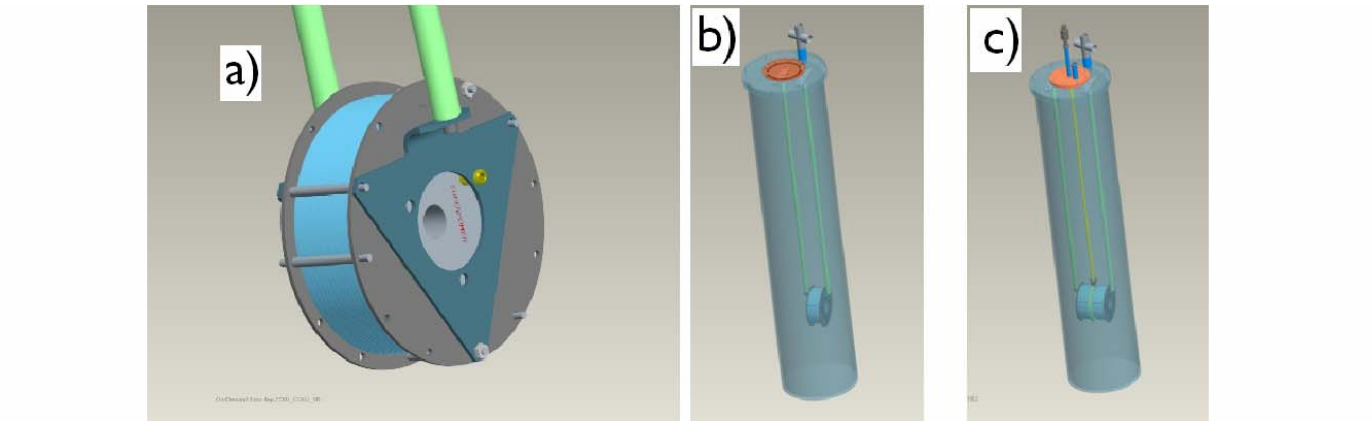

Figure 25: a) 14 pancake coils to be built and tested in FY 2009. b) on left shows a solenoid with 14 pancake coils to be built and tested inside the cryostat in FY09 and (c) on right shows 28 pancake coils (a 14-pancake coil on either side of a test sample) in FY10 as a part of the current SBIR Phase II .

PBL will design and build a quench protection system for the following combined systems.

BNL will then assemble each of these insert coils a) the YBCO 95 mm OD 12 T coil, and b) the Bi 2212 ~ 4 T coil inside the then existing [ref 27] 10 T YBCO coil with ID 10 cm and OD 165 mm

(being built under the active SBIR Phase II with Particle Beam Lasers, Inc.). Figure 23 shows, by colors, fields for the 12 T YBCO coil inside the 10 T one. BNL will then test both combined coil combinations at 4 K, at which temperature they should generate field approaching 14 T and 22 T respectively. They will also be tested at higher temperatures and lower fields. Figure 24a shows the expected axial fields for the case with YBCO coils as both insert and outsert.

e) Design and test of a hybrid magnet system approaching 40 T

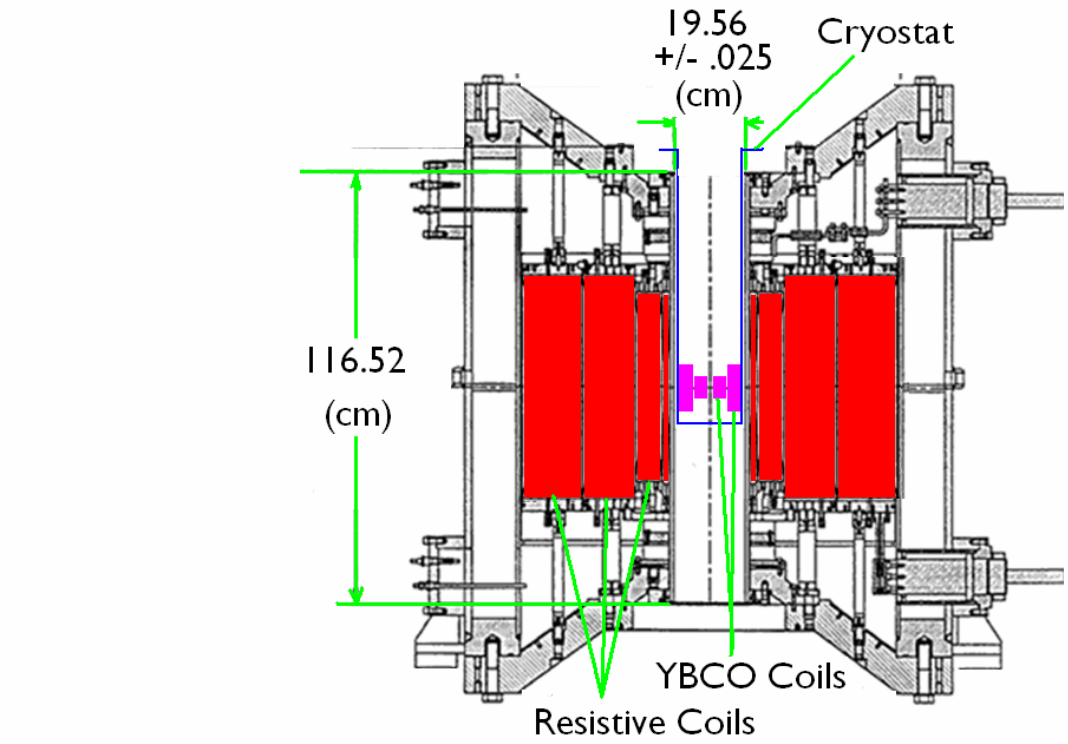

Figure 26: Cross section of the NHMFL 19 T resistive magnet with the 12T and 10T YBCO coils in their cryostat, inside the magnet.

PBL will also design a quench protection system for the following test.

BNL, together with PBL, will test one or both of the new coils (YBCO and Bi 2212), together with the YBCO 10 T [ref 27] outsert coil inside the background field from a 19 T Bitter coil at the NHMFL. In this test, the field on the axis should approach 40 T. Figure 24 b) shows an optimistic plot of the axial magnetic fields with the 12 T YBCO insert, 10 T YBCO outsert, and 19 T NHMFL resistive magnet. With the 4T Bi-2212 insert, 10 T YBCO outsert and 19 T NHMFL resistive magnet, fields approaching 33 T should be obtained at 4 K.
Figure 26 shows a cross section of the 19 T resistive magnet with the YBCO coils in their cryostat, inside the magnet.

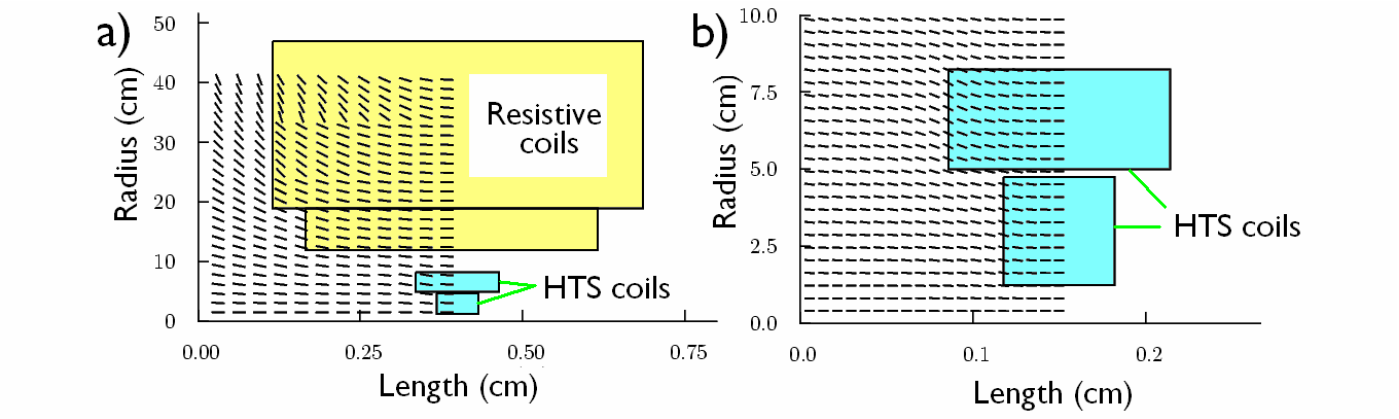

Figure 27: Field directions with 12 T YBCO insert and 10 T YBCO outsert inside the 19 T resistive magnet; a) shows all coils; b) shows detailed fields around the YBCO coils.

Figure 27 shows the field directions with both YBCO and the resistive magnet powered. It is seen that the field directions at the ends of the outer YBCO magnet are at small angles (≤18 deg) to the axis, but even such small angles will significantly reduce the current carried. Separate power supplies will be used to allow the end pancakes to run at lower currents than those in the center. The Bi-2212 coil halves may be mounted at the ends of the inner coil to straighten out the field lines. A detailed design will only be completed after the angular dependence of the chosen YBCO material is known. We have used the phrase "approaching 40 T" and other values, understanding that the angular dependence and other characteristics may limit the achieved fields. This is an experimental program – not a final design.

These tests will provide essential and valuable experience in operating such high field multiple coil designs that are needed prior to designing and testing 50 T coils. Since the design and construction of an all-superconducting 19 T solenoid would be fairly straightforward, then, if 40 T is achieved in this test, the practicality of an all-superconducting 40 T solenoid would be established. And if 40 T is not achieved, then valuable information on the real technical challenges of such a system will have been gained.

f) Further studies of all-superconducting 40-50 T solenoids

Using the experience from design and testing the 40 T hybrid magnet, the Phase II will study magnet and quench protection designs for 40-50 T systems. The use of YBCO and Bi-2223 will be studied, and compared with the Bi-2212 design described above. Optimization of magnet designs in the light of construction and material costs will be considered.

g) Staff and Consultant Responsibilities

Management of the project: Robert Weggel, PI; James Kolonko, Project Facilitator

Design and simulation of cooling in 40-50 T solenoids: Robert B Palmer

Study of recirculation of muons through one 50 T cooling stage: Alper Garren

Study of the use of this technology for other applications: David Cline

Design and optimization of 40-50 T solenoids: Robert Weggel

Oversight of BNL construction of YBCO coil and testing at BNL: Ramesh Gupta

Oversight of procurement of Bi-2212 coils from Oxford & integration with BNL: Ronald Scanlan

Oversight of the solenoid tests and measurements at NHMFL: Robert Weggel/Ramesh Gupta

IV) Phase II Work Plan and Schedule

a) Design and Simulation

Year #1

1- 6 months Start design matching and re-acceleration systems for earlier stages
6- 12 months Complete design matching and re-acceleration systems for earlier stages and consider the implications of using 40 T, instead of 50 T magnets.

Year #2

12- 18 months Complete the study including considerations of the effects of magnet errors
18- 24 months Report preparation

b) HTS Solenoid Schedule at BNL & NHMFL

Year #1

0 – 2 months Conceptual design studies
0 – 8 months Conductor testing (R&D samples and actual conductor)
1 – 4 months Overall and engineering design of the insert solenoid
3 – 6 months Coil tooling design and construction
4 – 5 months YBCO conductor received for insert solenoid
6 – 10 months Coil winding and individual LN2 coil tests
10 – 12 months Support structure fabrication and magnet assembly

Year #2

12 – 13 months	YBCO insert solenoid testing in a range of temperature (4K-77K)
12 – 13 months	Engineering design of the combined solenoid (insert and outsert)
13 – 14 months	YBCO combined solenoid testing (4K-77K)
13 – 14 months	BSCCO insert solenoid received
14 – 15 months	BSCCO insert and YBCO outsert solenoid testing (4K-77K)
15 – 16 months	Combined solenoid delivered to PBL for testing at NHMFL
22– 23 months	Report preparation

c) Quench Protection Circuit

Year #1 and Year #2

0 – 24 months	Design, fabricate, test, and install quench protection circuit for 50 T system.

V) ANTICIPATED PUBLIC BENEFITS

Possible Market for High-Field Nuclear Magnetic Resonance Magnets

The concept of NMR (Nuclear Magnetic Resonance) provides valuable information in many fields of science. The process of nuclei absorbing radio frequency resonant radiation in a static magnetic field is called NMR. The frequency of the resonance ώ goes like [28]

$$\omega \text{ proportional to } BM$$

where B is the static magnetic field and M is the nuclear magnetic moment. Most experiments to date have used B fields in the range of 5 to 10 T. To work in the higher B field region many experiments use pulsed magnetic fields. The resolution goes like $1/B^2$ [29]. An example is the recent experiment of D. Bobela and Taylor " Nuclear Magnetic Resonance Studies of Tellurium and Antimony Bonding in Crystal Sb_2Te_3 GeTe and Ge_2Sb_2 Te_5, Japanese Journal of Applied Physics 47, 10, 2008, pp 8162-8165. This experiment uses a 15T pulsed field and could possibly benefit from a DC 15T field or greater as is being proposed here. Currently no 40T magnets are available for commercial use either.

There is no general survey of the market for NMR magnets, but we have contacted Mark Bird at the FSU Magnet Laboratory for estimates. He writes "Kevin Smith worked for Oxford Instruments for 23 years as an engineering manager in various magnet groups. He joined us in May 2008. He says a few years ago the magnet market (excluding the spectrometers) was approximately 100M British pounds per year. Tim Cross provides some information below. If you want more detail, it is probably best to contact the leading NMR magnet builders: Varian and/or Bruker."

And Tim Cross writes: "I am afraid that I do not have a reasonable estimate of this global market and it is complicated by whether or not MRI is included. I know that in just two orders late last Fall Bruker for a total of $23M for NMR spectrometers up to 22.3 tesla."

While these estimates are very preliminary, it is our intention in our Phase II study to carry out a more detailed study of the possible market for 10T to 20T HTS magnets as are being proposed here for future NMR studies. We believe it is also possible to operate these magnets at the higher temperature of 35 K and to provide 5 – 10T magnets with relaxed cryogenic requirements. Both of these features could be of importance in future markets. We also hope to find sources of venture capital for PBL to be able to market these very high field magnets.

Some additional information on NMR studies are:

a) Probes of molecular structure [28]
b) Spectra of NMR in liquids [29] [30]
c) NMR studies on solids [31]
d) Two dimensional NMR studies [31]
e) Medical Imaging

VI) RESOURCES

a) Principal Investigator

Robert J. Weggel has had 40 years of experience as a magnet engineer and designer, first at the Francis Bitter National Magnet Laboratory at MIT and also at Brookhaven National Laboratory as well as extensive consulting experience in solenoid magnet design. In the course of his career he has authored over 100 peer-reviewed articles concerning resistive and superconducting magnets as well as hybrid high-field versions. He has had extensive experience optimizing magnets for various uses including solid state research, accelerator and medical applications. He has co-authored with D.B. Montgomery the book “Solenoid Magnet Design”.

b) Facilities and Equipment

The applicant has been successful in prior years obtaining SBIR grants and has experience complying with federal government grant guidelines and regulations and working with federal grant officers. The Phase II work described above will be carried out in leased office space in Los Angeles, the home office of the principal investigator in Reading, MA, and the home offices of the other PBL, Inc. employees and consultant. Company furnished computer hardware and public domain software will be used as appropriate. The company expects to reserve time and use the NHMFL in Tallahassee, FL for solenoid tests and measurements.

Facility and Resources in the Superconducting Magnet Division at Brookhaven National Laboratory

Construction and test of HTS solenoid will be carried out within a 55,000 square foot multipurpose R&D complex at Superconducting Magnet Division at BNL. The division has a staff of a total of about 50 persons, including scientists, engineers, technicians and administrative staff. It has been a

major player in the development of superconducting magnets for the last three decades. In addition, it has tested over 100 HTS tape and wire samples, built and tested over 50 HTS coils and over 10 HTS magnets. A prominent asset of the complex is a working cryogenic test facility, complete with high current, high resolution and high stability power supplies. The facility allows a variety of testing of superconductors, coils and magnets in a temperature range of ~2 K to ~80 K. In addition, among the various elements of dedicated equipment in the facility are several computer-controlled, automated coil winding machines, automated cycle curing and soldering stations, centralized exhaust vent systems, and hydraulic presses all of which are available for use in the construction of superconducting magnetic devices. The building is supported by several large capacity (15 ton minimum) overhead cranes. Finally, within the building complex are three machine shops with adequate capacity to manufacture the majority of components needed for the R&D task. For those items not able to be fabricated within the R&D facility, there are also onsite at BNL machine shop and a procurement group to handle orders with private companies.

BNL has developed, built and tested R&D HTS quadrupole magnets for FRIB, two types of HTS solenoids for the proposed electron cooling project, HTS R&D solenoid for MRI and common coil 2-in-1 R&D HTS dipole for a future hadron collider. Figure 28, top, shows the winding and finished HTS coils for the FRIB quadrupole. Figure 28, lower left, shows the 77 K Performance of the first series of coils made with first generation HTS. Lower right shows the performance of HTS coils in a magnet as a function temperature when two, four, six and twelve coils are energized in various configurations.

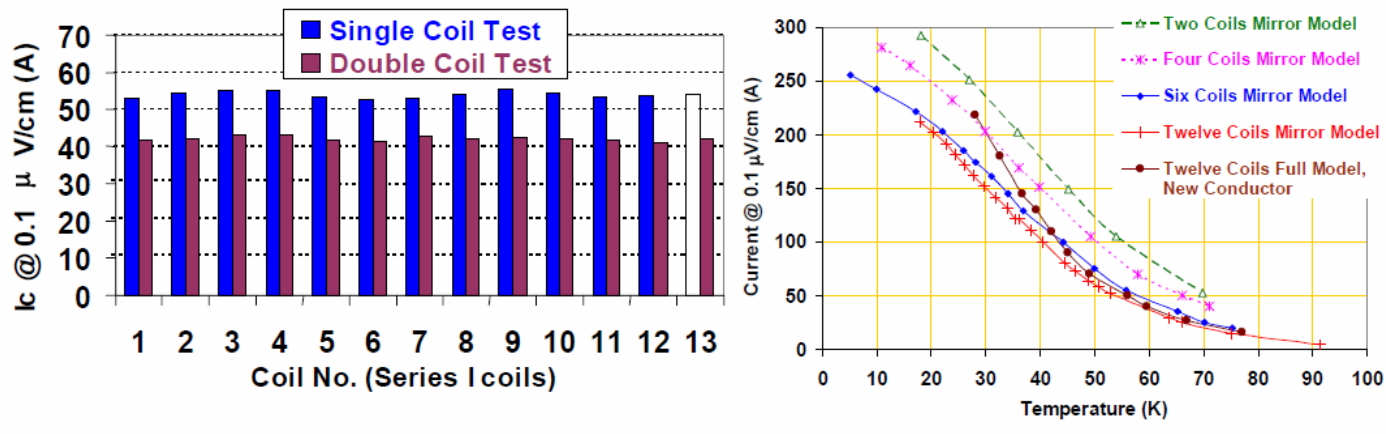

Figure 28: Top left: Winding of HTS quadrupole coil; Top right: Finished HTS coils; Lower left shows the 77 K Performance of the first series of coils made with first generation HTS. Lower right shows the performance of HTS coils in a magnet as a function temperature when two, four, six and twelve coils are energized in various configurations.

c) Consultants

Dr. David Cline is an internationally known experimental elementary particle physicist with expertise in the science and applications of particle accelerators and storage rings. Dr. Cline will serve as a consultant providing valuable input on physics issues connected with the cooling scheme and will continue to work on determining the use of such a system in commercial applications. A letter of commitment from Dr. Cline is part of this proposal.

d) Similar Grant Applications, Proposals, or Awards

Particle Beam Lasers, Inc. has no prior, current or pending support for a similar proposal and work.

VII) References

1. URL: http://lhc.web.cern.ch/lhc/

2. URL: http://www.linearcollider.org/cms/

3. URL: http://clic-study.web.cern.ch/clic%2Dstudy/

4. A.N. Skrinsky and V.V. Parkhomchuk, Sov. J. Part. Nucl. **12**, 223 (1981); D. Neuffer, Part. Accel. **14**, 75 (1983); R.B. Palmer et al., *A Practical High-Energy High-Luminosity mu+ mu- Collider,* Proc. Adv. Accel. Concepts: 6th Annual Conference, edited by P. Schoessow, AIP Conf. Proc. No. **335** (AIP, NY, 1995), p. 635.

5. M. D. Bird et al., *The Next Generation of Powered Solenoids at the NHMFL*, IEEE Trans. on Applied Superconductivity, Vol. 16-2 (2006), p. 973.

6. G.I. Budker, Proc. of the 7th International Conference on High Energy Accelerators, Yerevan, USSR 1969, edited by A.I. Alikhanian, p. 33; extract in Proc. of the Physics Potential & Development of mu+ mu- Colliders: Second Workshop, edited by D. Cline, AIP Conf. Proc. No. **352** (1996), p. 4.

7. A.N. Skrinsky, Proc. on the International Seminar on Prospects of High-Energy Physics, Morges (1971) unpublished; extract on Proc. of the Physics Potential & Development of mu+ mu- Colliders: Second Workshop (ref. 6), p. 6.

8. BNL Report No. BNL-52503 (1996), Fermilab Report No. Conf-96/092 (1996), LBNL Report No. LBNL-38946 (1996).

9. R.B. Palmer et al., *A Complete Scheme of Ionization Cooling for a Muon Collider*, PAC07 (2007) p. 3193.

10. J.S. Berg et al., *A Cost-Effective Design for a Neutrino Factory*, Phys. Rev. ST Accel. Beams **9**, 011001 (2006).

11. Y. Alexehin and E. Gianfelice-Wendt, Fermilab Report Beam-doc-2724-v1, 2007. URL: http://beamdocs.fnal.gov/AD-public/DocDB/DocumentDatabase.

12. H. G. Kirk, *Targetry for a u+u- Collider*, Proceedings of the 1999 Particle Accelerator Conference, New York, NY, March 1999, p. 3029.

13. S.A. Kahn et al., A High Field HTS Solenoid for Muon Cooling, PAC07, p. 446 (2007)

14. R. Fernow, PAC97 (1997), p. 3020; URL=http://pubweb.bnl.gov/people/fernow/icool/

15. R. Fernow, PAC97 (1997), p. 3020; URL=http://pubweb.bnl.gov/people/fernow/icool/

16. J. Norem et al., *Recent Results from the MuCool Test Area,* PAC07, (2007), p. 2239; *The MuCool rf Program*, EPAC 06, (2006), p. 1358

17. Y. Alexahin et al., *6D Iionization Cooling Channel with Resonant Dispersion Generation*, PAC07 (2007), p. 3477.

18. Y. Derbenev & R. Johnson, *Six-Dimensional Muon Cooling using a homogeneous absorber.*., Phys.Rev. ST Accel. Beams **8,** 041002 (2005); S. Kahn et al., *Magnet System for Helical Muon Cooling Channels*, PAC07 (2007), p. 443.

19. Y. Derbenev et al., Parametric Resonance Ionization Cooling and Reverse Emittance Exchange for Muon Collider, COOL05; D. Newsham et al., *Simulations of Parametric-Resonance Ionization Cooling*, PAC07 (2007), p. 2927. R. Johnson et al., *Low Emittance Muon Colliders*, PAC07 (2007), p. 706.

20. *Feasibility Study-II of a Muon-Based Neutrino Source*, ed., S. Ozaki, R. Palmer, M. Zisman, and J. Gallardo, BNL-52623 (2001). http://www.cap.bnl.gov/mumu/studyii/FS2-report.html

21. “Present and future applications for advanced superconducting materials in high field magnets”, A. Twin, J. Brown, F. Domptail, R. Bateman, R. Harrison, M. Lakrimi, Z. Melhem, P. Noonan, M. Field, S. Hong, K. Marken, H. Miao, J. Parrell, and Y. Zhang, IEEE Trans. Appl. Supercond., vol. 17, 2295-2298, 2007.

22. “Costs of high-field superconducting strands for particle accelerator magnets”, L.D. Cooley, A.K. Ghosh, and R.M. Scanlan, Supercond. Sci. Technol. **18** (2005) R51-R65.

23. Quench studies on a layer-wound $Bi_2Sr_2CaCu_2O_x$/AgX coil at 4.2 K, Trociewitz, U.P.; Czabaj, B.; Hong, S.; Huang, Y.; Knoll, D.C.; Larbalestier, D.C.; Markiewicz, W.D.; Miao, H.; Meinesz, M.; Wang, X. and Schwartz, J., Supercond. Sci. Technol., **21** (2), 025015 (2008).

24. “Progress in Wind-and-React Bi-2212 Accelerator Magnet Technology”, *A. Godeke, D. Cheng, D.R. Dietderich, C.R. Hanaford, S.O. Prestemon, G. Sabbi,* Lawrence Berkeley National Laboratory; *Y. Hikichi, J. Nishioka, T. Hasegawa,* SWCC Showa Cable Systems, paper 3LY03 presented at ASC 2008, Chicago, IL.

25. “Status of High Temperature Superconductor Magnet R&D at BNL,” R.Gupta et al., International Conference on Magnet Technology (MT-18), Morioka City, Japan (2003).

26. R.Gupta, recent quote from American Superconductor Corp., private communication.

27. Solenoid being constructed under the SBIR Phase II: “Development of a 6-Dimensional Muon Cooling System Using Achromat Bends and Design, Fabrication and Test of a Prototype High Temperature Superconducting (HTS) Solenoid for the System”.

28. Principles of Magnetic Resonance (Springer, New York, 1996) 3rd ed.

29. Becker, ED, High Resolution NMR Theory and Application, Academic Press, New York (1980)

30. Fyfe Solid State NMR for Chemists, CFC Press, Guelph, Ontario (1983)

31. Mehring, M. “High Resolution NMR of Solids”, Springer, Heidelberg (1981)